© 2024. Published by The Company of Biologists Ltd | Development (2024) 151, dev202870. doi:10.1242/dev.202870

RESEARCH ARTICLE

An updated model of shoot apical meristem regulation by ERECTA family and CLAVATA3 signaling pathways in *Arabidopsis*

Muhammad Uzair[1], Ricardo Andres Urquidi Camacho[2,*], Ziyi Liu[2], Alex M. Overholt[1], Daniel DeGennaro[1], Liang Zhang[1,‡], Brittani S. Herron[1], Tian Hong[1,2] and Elena D. Shpak[1,2,§]

ABSTRACT

The shoot apical meristem (SAM) gives rise to the aboveground organs of plants. The size of the SAM is relatively constant due to the balance between stem cell replenishment and cell recruitment into new organs. In angiosperms, the transcription factor WUSCHEL (WUS) promotes stem cell proliferation in the central zone of the SAM. WUS forms a negative feedback loop with a signaling pathway activated by CLAVATA3 (CLV3). In the periphery of the SAM, the ERECTA family receptors (ERfs) constrain *WUS* and *CLV3* expression. Here, we show that four ligands of ERfs redundantly inhibit the expression of these two genes. Transcriptome analysis confirmed that *WUS* and *CLV3* are the main targets of ERf signaling and uncovered new ones. Analysis of promoter reporters indicated that the *WUS* expression domain mostly overlaps with the *CLV3* domain and does not shift along the apical-basal axis in *clv3* mutants. Our three-dimensional mathematical model captured gene expression distributions at the single-cell level under various perturbed conditions. Based on our findings, CLV3 regulates cellular levels of *WUS* mostly through autocrine signaling, and ERfs regulate the spatial expression of *WUS*, preventing its encroachment into the peripheral zone.

KEY WORDS: *Arabidopsis*, Stem cells, ERECTA, EPFL, WUSCHEL, Shoot apical meristem

INTRODUCTION

In contrast to animals, plants generate very few organs during embryogenesis, with most of the organogenesis occurring after seed germination throughout the entire lifespan. New cells for aboveground plant organs are supplied by the shoot apical meristem (SAM) and axillary meristems. The SAM forms between cotyledons or embryonic leaves during embryogenesis. After germination, it generates the internodes, leaves and flowers of the main stem. The SAM is located at the apex of the main stem. Later in development, axillary meristems develop in the leaf axils and form branches (Wang, 2021). In all meristems, there is a small cluster of pluripotent slow-dividing stem cells in the center. Once cells are displaced from the center into the periphery, they grow and divide at a faster rate, differentiate, and ultimately are incorporated into organs. The molecular mechanisms controlling the transition of stem cells into differentiating cells of the peripheral zone are of fundamental interest to plant developmental biology. In the SAM, this transition relies on the ability of cells to communicate using a variety of extracellular signals (Demesa-Arevalo et al., 2024).

The homeobox transcription factor WUSCHEL (WUS) is essential for maintaining the SAM central zone in *Arabidopsis*. In the *wus* mutant, cells in the center differentiate prematurely, and the SAM disappears (Laux et al., 1996; Mayer et al., 1998). Ectopic and inducible expression of *WUS* promotes stem cell identity and increases the size of the central zone (Schoof et al., 2000; Yadav et al., 2010). Multiple signaling pathways regulate *WUS* expression. Cytokinins promote and position *WUS* expression along the apical-basal axis (Lindsay et al., 2006; Gordon et al., 2009; Chickarmane et al., 2012). A signaling pathway activated by the extracellular glycopeptide CLAVATA3 (CLV3) inhibits *WUS* expression. When CLV3 or its putative receptor CLAVATA1 (CLV1) are mutated, expression of *WUS* is increased (Clark et al., 1995, 1993; Schoof et al., 2000; Brand et al., 2000). In turn, WUS promotes the expression of *CLV3,* which leads to the formation of a negative feedback loop responsible for the stability of the SAM size (Schoof et al., 2000). In addition to *CLV3*, several other peptides encoded by the CLAVATA3-LIKE/ENDOSPERM SURROUNDING REGION (CLE) gene family, such as CLE16, CLE17 and CLE40, have been shown to regulate the size of the SAM (Dao et al., 2022; Schlegel et al., 2021).

Recently, we have demonstrated that in addition to CLV3 and CLE peptides, another signaling pathway controls *WUS* expression (Zhang et al., 2021). In *Arabidopsis*, three plasma membrane receptors, ERECTA (ER), ERECTA-LIKE1 (ERL1) and ERL2, redundantly regulate the width of the vegetative SAM and promote leaf initiation in its periphery (Chen et al., 2013; Uchida et al., 2013). Collectively, these receptors are called ERECTA family receptors (ERfs). In the SAM, ERf activity is controlled by four extracellular proteins – EPFL1, EPFL2, EPFL4 and EPFL6 (herein collectively referred to as EPFLs) – that are expressed in the SAM periphery (Kosentka et al., 2019). Genetic analysis has demonstrated that ERfs and CLV3 function synergistically in controlling SAM size and organogenesis in the peripheral zone (Zhang et al., 2021; Kimura et al., 2018). The *clv3 er erl1 erl2* mutant forms a gigantic meristem that cannot form leaves or internodes (Zhang et al., 2021). Our previously published data show that *wus* is epistatic to genes encoding ERfs (Zhang et al., 2021). Stimulation of ERf signaling with exogenous EPFL4 or EPFL6 rapidly decreases both *CLV3* and *WUS* expression. Based on these data, we have proposed that ERfs restrict the width of the central zone in the SAM by inhibiting the expression of *CLV3* and *WUS* in the peripheral zone (Zhang et al., 2021).

The main focus of the current investigation is the role of EPFL and CLV3 signaling pathways in SAM maintenance and

[1]Department of Biochemistry, Cellular and Molecular Biology, University of Tennessee, Knoxville, TN 37996, USA. [2]UT-ORNL Graduate School of Genome Science and Technology, University of Tennessee, Knoxville, TN 37996, USA. *Present address: Department of Biology, University of Pennsylvania, Philadelphia, PA 19104, USA. ‡Present address: Complex Carbohydrate Research Center, University of Georgia, Athens, GA 30602, USA.

§Author for correspondence (eshpak@utk.edu)

R.A.U.C., 0000-0002-5526-3938; T.H., 0000-0002-8212-7050; E.D.S., 0000-0002-5702-7517

Handling Editor: Dominique Bergmann
Received 15 March 2024; Accepted 16 May 2024

Development (2024) 151, dev202870. doi:10.1242/dev.202870

organogenesis. We studied the role of EPFLs in the regulation of *CLV3* and *WUS* expression and uncovered that the four EPFL ligands function redundantly. Using RNA sequencing (RNAseq), we analyzed gene expression changes after a brief activation of ERf signaling with EPFL6. This experiment confirmed that *CLV3* and *WUS* are the main targets of the pathway and uncovered several new potential targets. In addition, we studied the role of CLV3 in the control of *WUS* expression. Whereas it is broadly accepted that CLV3 prevents *WUS* expression in the top layers of the meristem, our analysis indicated that CLV3 regulates the amount of *WUS* per cell and not its spatial expression. Finally, the role of EPFL signaling in leaf organogenesis was studied using the DORNROSCHEN (DRN; also known as ENHANCER OF SHOOT REGENERATION 1, ESR1) and DRN-LIKE (DRNL; also known as ENHANCER OF SHOOT REGENERATION 2, ESR2) markers. DRN and DRNL are transcription factors belonging to the APETALA2/Ethylene Responsive Factor (AP2/ERF) gene family. DRNL is a direct target of auxin and one of the first markers of organ initiation (Chandler et al., 2011; Comelli et al., 2016; Dai et al., 2023). Whereas DRN is normally expressed in the central zone, it is upregulated in the incipient primordia when DRNL is absent (Dai et al., 2023; Kirch et al., 2003). Our experiments indicated that although cells designated to become leaf primordia are specified in the peripheral zone, the bulging of the primordia is inefficient when ERf signaling is disrupted.

RESULTS

EPFL1, *EPFL2*, *EPFL4* and *EPFL6* redundantly control expression of *WUS* and *CLV3*

EPFL1, EPFL2, EPFL4 and EPFL6 redundantly restrict the size of the SAM (Kosentka et al., 2019). When EPFL4 and EPFL6 are supplied exogenously, they suppress *WUS* and *CLV3* expression (Zhang et al., 2021). To test whether EPFL1 and EPFL2 also regulate the expression of *WUS* and *CLV3*, we analyzed the spatial expression of *CLV3* and *WUS* in the vegetative SAM of *epfl* mutants using previously described H2B-GFP reporters (Zhang et al., 2021). Seedlings at 3 days post germination (3DPG) were used for all experiments. The reporter analysis showed that simultaneous knockout of either *EPFL4* and *EPFL6* or *EPFL1* and *EPFL2* had a minimal effect on the spatial expression pattern of *CLV3* and *WUS* (Fig. 1A-D). We observed only a minute increase in the height of the *WUS* domain in *epfl1 epfl2* (*epfl1,2*) and *epfl4 epfl6* (*epfl4,6*) mutants (Fig. 1A,B) and a very slight broadening of *CLV3* in the L1 layer of the *epfl1,2* mutant (Fig. 1C,D). The small increase in *CLV3* expression in the *epfl1,2* mutant correlated with a slightly broader SAM (Fig. 1E). Next, we analyzed the expression of *CLV3* and *WUS* in *epfl1/+ epfl2 epfl4 epfl6* (*epfl1/+,2,4,6*) and *epfl1 epfl2 epfl4 epfl6* (*epfl1,2,4,6*) quadruple mutant seedlings. In the seedlings heterozygous for *epfl1* mutations, the sizes of *CLV3* and *WUS* domains were slightly increased compared to those in both the wild type and double mutants (Fig. 1A-D). Again, this correlated

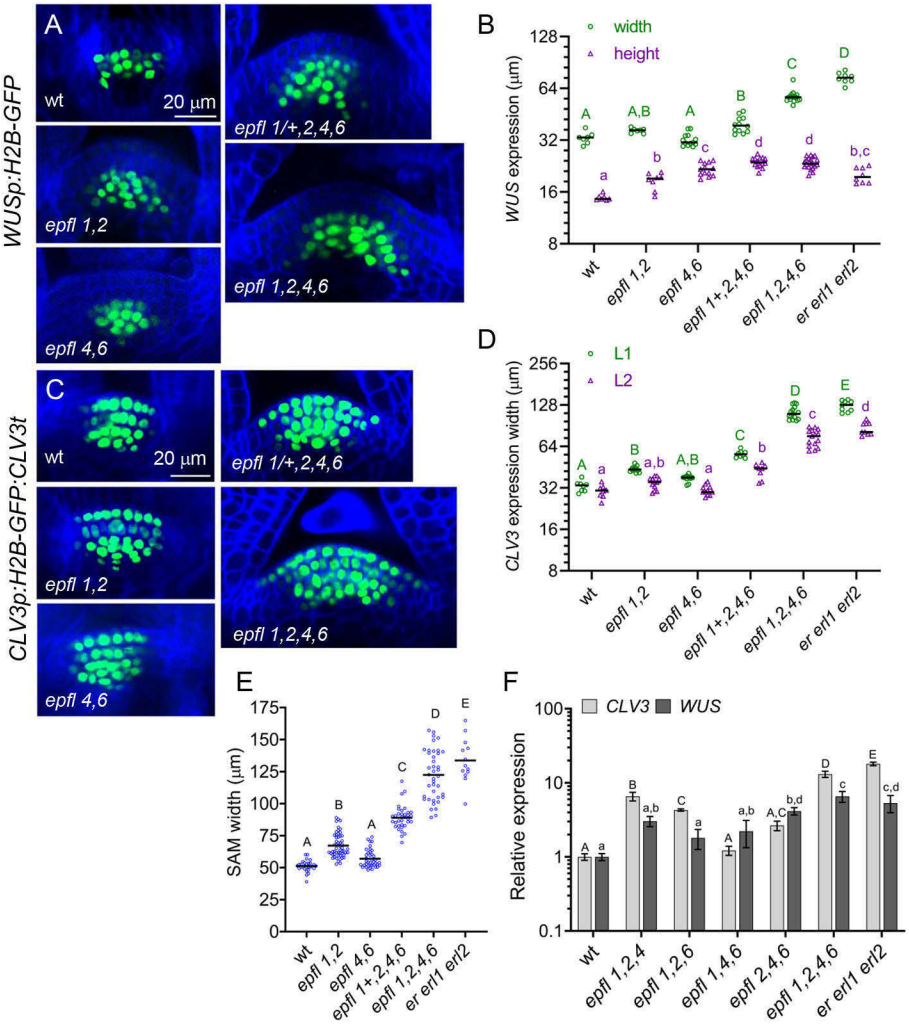

Fig. 1. Genes encoding EFPLs synergistically regulate the expression of *CLV3* and *WUS*. (A,C) Representative confocal images of the SAM region of 3DPG seedlings of the indicated genotypes (wt, wild type) transformed with promoter reporters for (A) *WUS* (*WUSp:H2B-GFP*; green) or (C) *CLV3* (*CLV3p:H2B-GFP:CLV3t*; green). All images are in the same panel are shown at the same magnification. The cell walls were stained with SR2200 (blue). (B) The width and height of the *WUS* expression region in seedlings of the indicated genotype, as shown by the H2B-GFP promoter reporter. *n*=7-20. (D) The width of *CLV3* expression in the L1 and L2 layers for the indicated genotypes, as shown by the H2B-GFP promoter reporter. *n*=8-15. (E) Comparison of the SAM width at 3DPG for the indicated genotypes. *n*=13-54. Measurements in B, D and E were taken from confocal images. (F) RT-qPCR analysis of *WUS* and *CLV3* in 3DPG seedlings of the indicated genotypes. *n*=3. Bars in B, D and E show the mean. Data in F are shown as the mean±s.d. Statistical differences were detected using a one-way ANOVA followed by a Tukey post-hoc test with $P<0.05$; letters denote statistically significance differences, with no statistically significant difference between groups marked by the same upper- or lower-case letter.

Development (2024) 151, dev202870. doi:10.1242/dev.202870

with a subtle increase in the SAM width (Fig. 1E). In the quadruple *epfl1,2,4,6* mutant, the width of *WUS* and *CLV3* expression domains and the SAM were the most significantly increased (Fig. 1A-E). These experiments indicate that all four ligands regulate the expression of *WUS* and *CLV3* in a mostly redundant manner.

At the same time, there were subtleties in the contribution of individual EPFLs to the regulation of these two genes. When we analyzed the expression of *WUS* and *CLV3* in *epfl* triple and quadruple mutants using reverse transcription-quantitative PCR (RT-qPCR), we observed increased expression of these two genes, and the mutant combination dictated which one was upregulated more (Fig. 1F). The experiment suggests that EPFL1 and EPFL2 might have a more significant role in the regulation of *CLV3* whereas EPFL4 and EPFL6 are more important for the regulation of *WUS*. In addition, a comparison of *epfl1,2,4,6* and *er erl1 erl2* mutants identified some differences: in the *epfl1,2,4,6* mutant, *CLV3* and *WUS* were expressed in a narrower domain (Fig. 1B,D), *CLV3* was expressed at a lower level (Fig. 1F) and the SAM was slightly narrower (Fig. 1E). This suggests that either ERfs can weakly regulate the SAM in a ligand-independent manner or additional EPFL ligands contribute to the regulation of the SAM structure.

Transcriptome analysis identifies several meristematic genes, including *CLV3* and *WUS*, as the immediate targets of EPFL6

A previous study in which transient activation of ERfs with EPFL4 and EPFL6 was followed by RT-qPCR identified *CLV3* and *WUS* as downstream targets (Zhang et al., 2021). To discover targets of ERf signaling using an unbiased approach, we performed transcriptome sequencing. As we were specifically interested in the meristematic targets, many of which are expressed at low levels, we used *clv3 epfl1,2,4,6* seedlings that have very large vegetative SAMs (Zhang et al., 2021) and performed a relatively deep sequencing (>50 M reads per sample). We treated 3DPG seedlings exogenously with 10 µM EPFL6 for 3 h with and without 10 µM cycloheximide (CHX). CHX was used to test whether the regulation of gene expression by EPFL6 depends on translation. Based on principal component analysis (PCA), the obtained RNAseq data clustered according to treatment and showed a high degree of intra-treatment reproducibility (Fig. S1A). A Pearson correlation heatmap of replicates also indicated the similarity between biological replicates (Fig. S1B). In the samples treated with EPFL6 only, we observed minimal changes in gene expression compared to the mock treatment (Fig. S1A,B). In response to EPFL6 alone, eight genes were upregulated by at least 1.5-fold, or 0.585 $\log_2$ fold change (LFC), and fourteen genes were downregulated at least −0.585 LFC. All results were corrected for multiple comparisons and had a false discovery rate (FDR) of less than 0.05 (Table S1). The RNAseq data from plants treated with CHX or with CHX and EPFL6 (CHX+EPFL6) clustered together but were not as similar. As expected, global inhibition of translation by CHX led to widespread dysregulation of gene expression in the mock sample (Table S1). Downregulated and upregulated targets of EPFL6-only treatment showed no coordinated expression pattern under CHX-only treatment (Fig. 2B). Using the

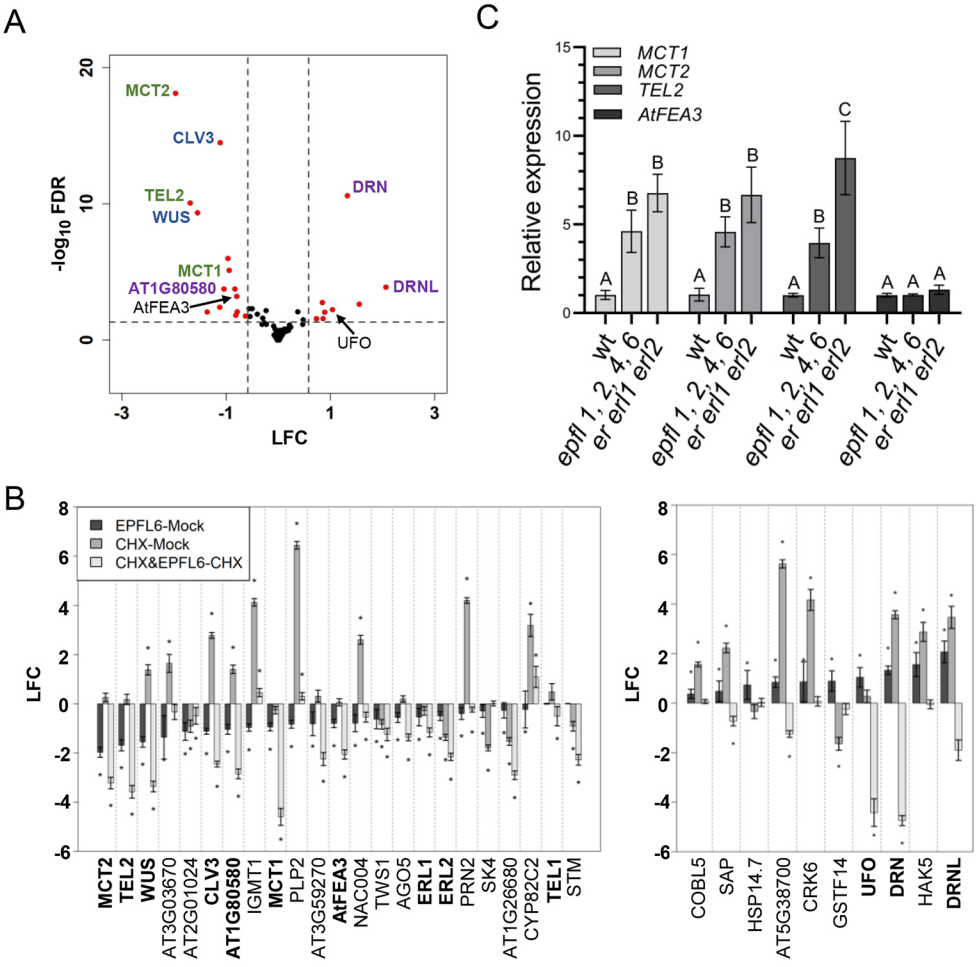

Fig. 2. Downstream targets of EPFL6 based on RNAseq analysis. (A) A volcano plot shows changes in gene expression in 3DPG *clv3 epfl1,2,4,6* seedlings after treatment with 10 µM EPFL6. Vertical dashed lines indicate an LFC cutoff of ±0.585; horizontal dashed lines mark the FDR cutoff of 0.05. Selected genes that are discussed in the manuscript are indicated. Blue indicates genes studied previously. Two groups of paralog genes are indicated by green and purple. (B) Comparison of changes in gene expression in response to 10 µM EPFL6 (versus mock treatment; EPFL6-Mock), 10 µM CHX (versus mock treatment; CHX-mock) and CHX+EPFL6 cotreatment versus only CHX treatment (CHX&EPFL6-CHX). Most genes downregulated in response to EPFL6 are also downregulated in response to CHX+EPFL6 (left panel). None of the genes upregulated in response to EPFL6 are upregulated in response to CHX+EPFL6 (right panel), suggesting that their upregulation is indirect. Genes discussed in the text are in bold. *FDR<0.05. Data are presented as the mean±s.e.m. of *n*=3 replicates. (C) RT-qPCR analysis of selected gene expression in 3DPG seedlings of the indicated genotypes (wt, wild type). Data are presented as the mean±s.d. of *n*=3. Statistical differences were detected using a one-way ANOVA followed by a Tukey post-hoc test with $P<0.05$; letters denote statistically significance differences, with no statistically significant difference between groups marked by the same letter.

Development (2024) 151, dev202870. doi:10.1242/dev.202870

CHX treatment as a control, we analyzed CHX+EPFL6-induced changes and observed a reduction of gene expression for both genes downregulated and upregulated by EPFL6 alone (Table S1). This suggests that most of these genes are directly repressed by the ERf signaling pathway.

Consistent with our previously published data (Zhang et al., 2021), RNAseq showed ∼50% downregulation of *CLV3* and *WUS* expression in response to EPFL6 treatment (Fig. 2A). The reduction in *WUS* and *CLV3* expression was independent of the production of new proteins, as we observed their downregulation in samples treated simultaneously with EPFL6 and CHX (Fig. 2B). These experiments confirmed that *WUS* and *CLV3* are direct targets of the ERf signaling pathway.

Additionally, we found that genes encoding three members of the MEI2 family of RNA-binding proteins – *MEI2 C-TERMINAL RRM ONLY LIKE1* (*MCT1*), *MCT2* and *TERMINAL EAR-LIKE 2* (*TEL2*) – were significantly downregulated by EPFL6 treatment (Fig. 2A,B). The expression of the fourth member of this family, *TEL1*, was slightly reduced by CHX+EPFL6 treatment but not by EPFL6 alone (Fig. 2B). Another gene downregulated by EPFL6 treatment was that encoding the leucine-rich-repeat protein AT3G25670 (hereafter referred to as AtFEA3), one of three *Arabidopsis* homologs of maize *FASCIATED EAR 3* (*FEA3*), which regulates the SAM size (Je et al., 2016). RT-qPCR analysis *of er erl1 erl2* and *epfl1,2,4,6* seedlings detected increased expression of *MCT1*, *MCT2* and *TEL2*, which is consistent with their downregulation by ERfs (Fig. 2C). We could not detect *TEL1* expression consistently in either the wild type or the mutants due to its extremely low expression, if any. There was no change in *AtFEA3* expression in the mutants (Fig. 2C), suggesting that it might not be a significant target of EPFLs. Finally, of note is the downregulation of *ERL1* and *ERL2* expression by EPFL6 (Fig. 2B and Table S1). Previously published data show that ERf signaling negatively regulates *ERL1* and *ERL2* expression (Pillitteri et al., 2007).

Out of ten genes upregulated in response to EPFL6, none were upregulated when EPFL6 was applied with CHX, suggesting that upregulation of these genes is an indirect response to EPFL6. The two upregulated genes with the lowest FDR were *DRN* and *DRNL* (Fig. 2A), which encode transcription factors that regulate meristem maintenance and organ initiation (Kirch et al., 2003; Ikeda et al., 2021, 2006). However, both of these genes were downregulated by EPFL6 in the presence of CHX (Fig. 2B, right panel, CHX&EPFL6-CHX bars). In addition, EPFL6 downregulated expression of the gene encoding AT1G80580, a close paralog of DRN and DRNL (Fig. 2A,B). This result suggests that EPFLs might downregulate this gene family directly while simultaneously indirectly promoting *DRN* and *DRNL* expression. EPFL6-only treatment upregulated the expression of *UNUSUAL FLORAL ORGANS* (*UFO*) (Fig. 2A), another meristematic gene (Long and Barton, 1998). However, in CHX+EPFL6 treatment, we observed the downregulation of *UFO* (Fig. 2B), suggesting that EPFL6 regulates the expression of this gene in a complex manner.

EPFL2 is expressed in the boundaries between the SAM and forming primordia (Kosentka et al., 2019). To test whether EPFL2 can alter the expression of genes identified by transcriptomics from the boundary, we created *epfl1,2,4,6* transgenic plants with inducible *EPFL2* expression (*epfl1,2,4,6*^{T}). We used the pOp/LhGR system that allows tissue-specific expression of a gene of choice in response to dexamethasone (DEX) (Samalova et al., 2005). The construct was created in such a way that in response to DEX, expression of *EPFL2* and *H2B-GFP* was induced in tissues where the *EPFL2* promoter was active (Fig. S2). Without induction, H2B-GFP could not be detected by confocal microscopy, but after 7 h of induction, H2B-GFP was clearly visible in the boundary zone of the SAM (Fig. 3A). Interestingly, RT-qPCR indicated that both *H2B-GFP* and *EPFL2* were expressed in transgenic plants without induction (Fig. 3B,C). After induction, their expression increased slightly. This suggests that our construct led to a leaky, unspecific expression at very low levels throughout the plant. This expression did not noticeably alter the phenotype of the *epfl1,2,4,6* mutant (data not shown). In response to DEX, expression of GFP, and presumably of EPFL2, was strongly activated in cells where the *EPFL2* promoter functions (Fig. 3A). Because this happens in very few cells out of many, RT-qPCR barely detected any change. Expression of *CLV3, MCT1*, *MCT2* and *TEL2* genes in transgenic seedlings without induction (*epfl1,2,4,6*^{T}-mock) was similar to their expression in untransformed *epfl1,2,4,6* seedlings (Figs 1FD, 2CD and 3D). When DEX was used to induce *EPFL2* expression for 7 h in the boundary of the SAM, expression of *CLV3, MCT1* and *MCT2* decreased (Fig. 3D). *TEL2* might be a specific target of EPFL4 and EPFL6. Unexpectedly, very low broad expression of *EPFL2* reduced the expression of *WUS* in *epfl1,2,4,6*^{T} seedings without induction to levels that were only slightly above the wild-type levels (Fig. 3E). Induction of *EPFL2* expression in the boundary did not significantly lower *WUS* expression. In summary, this experiment confirmed that *CLV3, MCT1* and *MCT2* are endogenous targets of EPFL2.

The expression patterns of *DRN* and *DRNL* are altered in the *epfl1,2,4,6* mutant

ERf signaling plays an important role in the initiation of cotyledons and leaves. However, the molecular mechanism is unknown (Chen et al., 2013; DeGennaro et al., 2022). Based on the role the AP2/ERF family plays in cotyledon and leaf initiation in a variety of species (Chandler et al., 2007; Capua and Eshed, 2017; Kusnandar et al., 2021) and on our RNAseq data, we hypothesized that ERfs might regulate organogenesis through control of *DRN* and/or *DRNL* expression. To test this hypothesis, we compared the expression of their H2B-GFP reporters in the wild type and *epfl* mutants. We used a 4.9 kb sequence upstream of the start codon and a 1.4 kb sequence downstream of the stop codon to analyze *DRN* expression. These regulatory regions have been reported to reflect the *DRN* expression similarly to RNA *in situ* hybridization (Kirch et al., 2003; Luo et al., 2018). To analyze *DRNL* expression, we used a 4.3 kb region upstream of the start codon as a promoter. The expression pattern of this regulatory region has also been tested previously and is consistent with RNA *in situ* hybridization (Luo et al., 2018). Based on published data, *DRN* is expressed in the young leaf primordia and the L1 and L2 layers (called the tunica) of the vegetative SAM (Kirch et al., 2003). *DRNL* is expressed in leaf and flower primordia (Ikeda et al., 2006; Nag et al., 2007). During flower development, *DRNL* is expressed in the primordia founder cells before the formation of auxin maxima and in the outer periphery of the future auxin peak (Luo et al., 2018; Chandler and Werr, 2014).

In agreement with published data, we observed expression of the *DRN* H2B-GFP reporter (*DRNp:H2B-GFP*) in the tunica of the wild-type SAM (Fig. 4A). In the L1 layer, the reporter was expressed broadly. In the L2 layer and deeper tissues, expression was narrow and correlated with the formation of leaf primordia. We observed a similar pattern in *epfl1,2* and *epfl1/+,2,4,6* seedlings, with the exception that, because the SAM in these mutants is slightly broader, *DRN* was expressed in a wider area of the L1 layer (Fig. 4B), and the correlation of *DRN* expression in L2 and L3 layers with forming organ primordia was more obvious. Even though the SAM of the *epfl1,2,4,6* mutant forms very few primordia, *DRN* was found to be

Development (2024) 151, dev202870. doi:10.1242/dev.202870

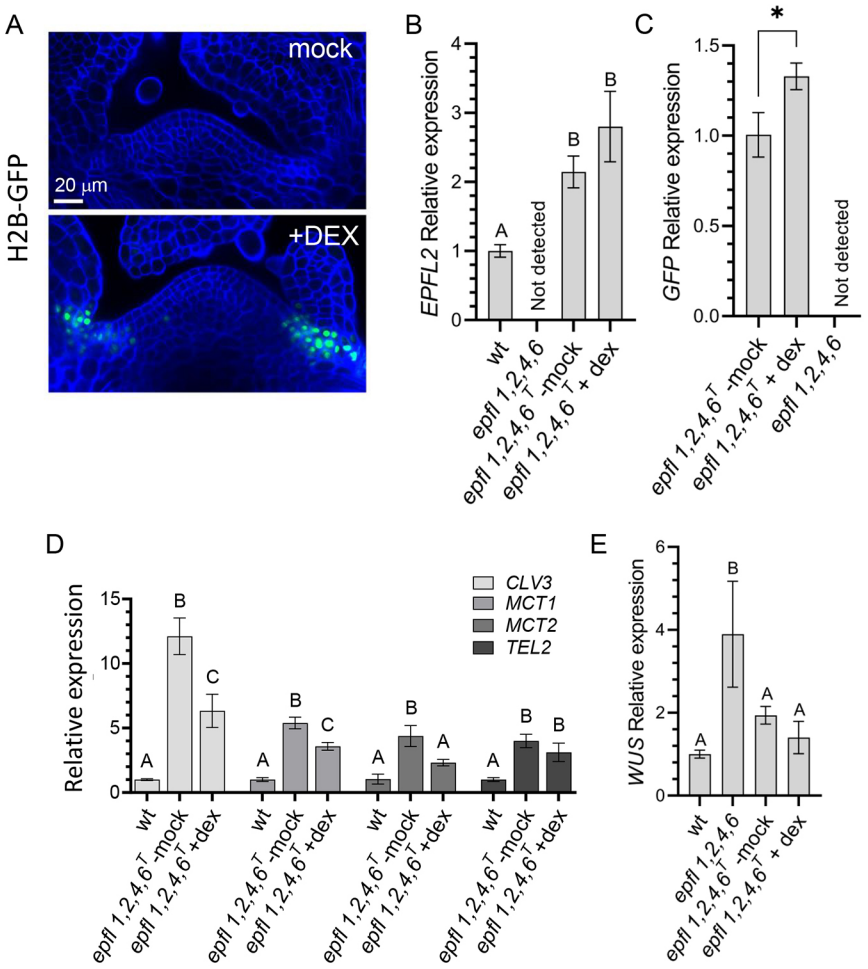

Fig. 3. Induction of EPFL2 in the SAM boundary leads to decreased expression of *CLV3*, *MCT1* and *MCT2*. (A) Confocal images of 3DPG *epfl1,2,4,6*^{T} seedlings following mock treatment or DEX treatment for 7 h. The seedlings express H2B-GFP (green) under the *EPFL2* promoter in response to DEX. Both images were acquired with the same magnification, and the same settings were used for confocal microscopy. The cell walls were stained with SR2200 (blue). Images are representative of ten seedlings. (B-E) RT-qPCR analysis of (B) *EPFL2*; (C) *H2B-GFP*; (D) *CLV3*, *MCT1*, *MCT2* and *TEL2*; and (E) *WUS* expression in (B,D,E) 3DPG wild-type (wt) seedlings, (B,C,E) 3DPG *epfl1,2,4,*6 seedlings and (B-E) 3DPG *epfl1,2,4,6*^{T} seedlings expressing inducible EPFL2 and H2B-GFP under the *EPFL2* promoter, with either mock treatment or DEX treatment as indicated. Data are presented as the mean±s.d. of *n*=3. Statistical differences were detected using a one-way ANOVA followed by a Tukey post-hoc test with $P<0.05$; letters denote statistically significance differences, with no statistically significant difference between groups marked by the same letter. *$P<0.05$ in C.

expressed very broadly in the L2 and L3 layers of this mutant. Because *DRN* is induced by auxin (Cole et al., 2009), and in the absence of ERf/EPFL signaling, auxin is present at higher levels in the SAM (DeGennaro et al., 2022), it is not clear whether the broader *DRN* expression observed in the SAM is related to altered auxin levels or whether ERf signaling directly downregulates this gene.

In the wild type, *DRNL* was expressed in the narrow strip of primordia founder cells (Fig. 4C). The *epfl1,2,4,6* mutant forms leaf primordia very inefficiently (Kosentka et al., 2019). Unexpectedly, we observed efficient expression of *DRNL* in the SAM of this mutant, suggesting that in the mutant founder cells of leaf primordia are specified. This result indicates that ERf signaling promotes the subsequent step of leaf primordia outgrowth. In addition, we observed broader *DRNL* expression. Whereas the width of the *DRNL* expression in the wild type was 2-3 cells, in the *epfl1,2,4,6* mutant, it was in the range of 4-7 cells. In the mutant, *DRNL* was also expressed in the L1 layer of the central zone. The *DRNL* promoter region contains auxin-responsive elements (Comelli et al., 2016). The broader expression of *DRNL* in the *epfl1,2,4,6* mutant could be either a direct consequence of the altered ERf signaling or due to changes in auxin accumulation.

In summary, analysis of *DRN* and *DRNL* reporters in *epfl* mutants demonstrated a broader expression of these genes. This result is consistent with the downregulation of these genes we observed upon CHX+EPFL6 treatment. However, this change could also result from increased auxin accumulation in the SAM of plants with mutation of genes encoding ERfs or EPFLs. DRN and DRNL have been linked with the induction of leaf initiation (Chandler et al., 2007). Our data suggest that our original hypothesis that ERfs promote leaf initiation through induction of *DRN* and *DRNL* was incorrect. Whereas increased expression of *DRN* and *DRNL* in the SAM of the *epfl1,2,4,6* mutant might alter some aspects of meristem maintenance, it is unlikely to inhibit leaf initiation. We speculate that ERfs do not specify the primordia founder cells but promote the outgrowth of demarcated leaf primordia.

Regulation of *WUS* expression by CLV3 signaling

In our previous work, we observed expression of *WUS* directly under the L2 layer in the wild-type vegetative SAM (Zhang et al., 2021). This contradicts the widely used description of *WUS* expression in the deeper layers of the SAM, only partially overlapping with *CLV3* expression (Truskina and Vernoux, 2018; Uchida and Torii, 2019; Fuchs and Lohmann, 2020; Han et al., 2020a; Hirakawa, 2021; Lopes et al., 2021; Shimotohno, 2022; Ince and Sugimoto, 2023), based on early studies of this gene (Schoof et al., 2000; Brand et al., 2000). To determine the *WUS* expression domain, we performed further analysis using promoter reporters for *WUS* and *CLV3*.

Identification of cell layers on two-dimensional images of the SAM can be misleading because the meristem is often sectioned at an oblique angle (Fig. S3A). During the analysis of *WUS* expression, we realized that unless we examined a three-dimensional (3D) image, we often erroneously detected *WUS* in deeper tissue layers than it was actually expressed (Fig. S3B,C). Thus, we carefully analyzed *z*-stacks of *WUS* and *CLV3* H2B-GFP reporter expression in the wild type, the

Development (2024) 151, dev202870. doi:10.1242/dev.202870

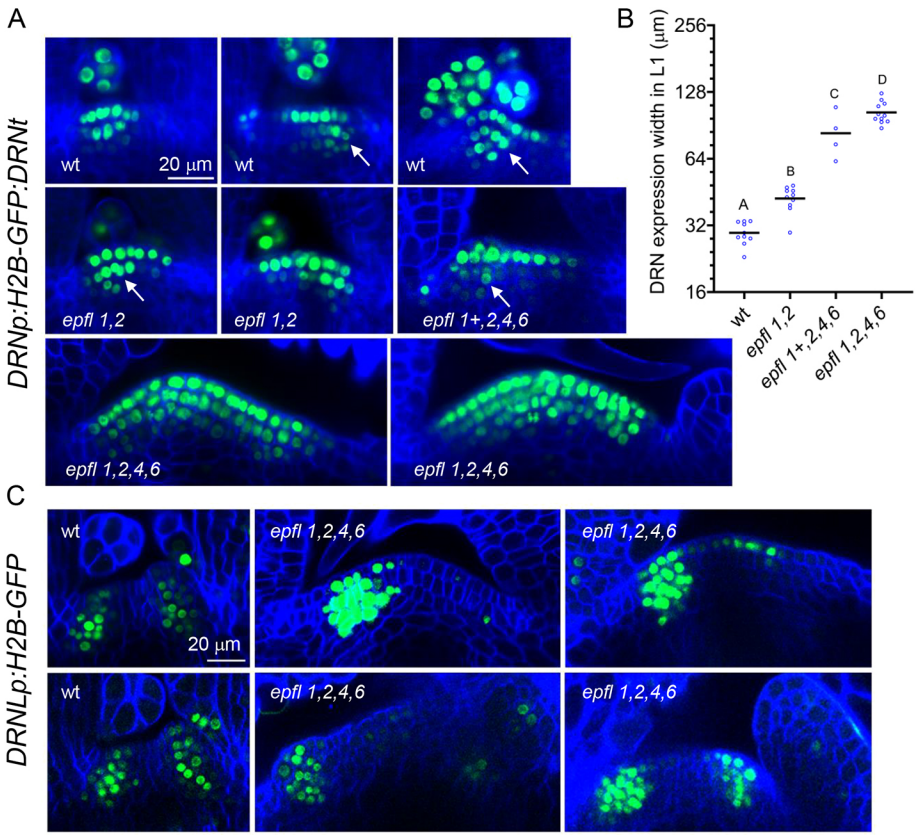

Fig. 4. Broader expression of *DRN* and *DRNL* in the SAM of *epfl* mutants. (A,C) Representative confocal images of the SAM region of 3DPG seedlings of the indicated genotypes (wt, wild type) expressing a promoter reporter construct for (A) *DRN* (*DRNp:H2B-GFP:DRNt*; green) or (C) *DRNL* (*DRNLp:H2B-GFP*; green). White arrows in A indicate the induction of *DRN* in incipient leaf primordia. All images in the same panel are shown at the same magnification. The cell walls were stained with SR2200 (blue). Images are representative of 20 seedlings. (B) The average width of *DRN* expression in the L1 layer of the SAM was measured on the confocal images. Bars indicate the mean; n=4-11 seedlings. Statistical differences were detected using a one-way ANOVA followed by a Tukey post-hoc test with P<0.05; letters denote statistically significant differences.

er erl1 erl2 mutant and the *clv3* mutant. In all images and in all seedlings, *WUS* was expressed in the third cell layer from the top at a constant distance from the surface of the SAM (Fig. 5D-G). In the *clv3* mutant, we never detected a shift of *WUS* upward, only a slight expansion of *WUS* downward. In the wild type, *WUS* was mostly expressed in two cell layers, whereas in the *clv3* mutant, *WUS* was sometimes expressed in three or four layers (Fig. 5D,E). In the *clv3 er erl1 erl2* mutant, *WUS* was primarily expressed in layers three and four from the top, with only occasional expression in deeper layers (Fig. 6). Interestingly, *WUS* expression was discontinuous in this mutant, although all cells, based on *CLV3* expression, were a part of the central zone (Fig. 6). In the *clv3* mutant, *er erl1 erl2* mutant and *clv3 er erl1 erl2* mutant, we observed much broader expression of *WUS* along the radial axis (Figs 5D,E and 6; Zhang et al., 2021). Thus, CLV3 and ERf signaling mainly regulate *WUS* expression along the radial axis of the SAM and not the apical-basal axis.

In the vegetative SAM, *CLV3* is expressed in the top 4-5 layers, and the depth of its expression is not altered in *clv3* and *er erl1 erl2* mutants (Fig. 5A-C) (Zhang et al., 2021). Thus, in the wild type, expression of *CLV3* and *WUS* strongly overlaps. All cells that express *WUS* also express *CLV3*. This means that CLV3 should inhibit *WUS* expression primarily through autocrine signaling, with *WUS*-expressing cells secreting CLV3 and the same cells sensing it. Paracrine signaling with CLV3 being secreted by L1 and L2 cells and sensed by L3 cells might also contribute to the regulation of *WUS* expression, but we speculate that the diffusion of CLV3 from the above layers will probably provide only a small fraction of the available ligand.

To understand how ERfs and CLV3 regulate *WUS* expression, we estimated the amount of *WUS* per cell. The *z*-stacks were used to calculate the number of cells expressing *WUS* in the wild type and the mutants (Fig. 5I; Movies 1, 2 and 3). Compared to the wild type, there were approximately six and five times more *WUS*-expressing cells in the *clv3* mutant and *er erl1 erl2* mutant, respectively. RT-qPCR was used to determine the difference in *WUS* expression (Fig. 5H). After the difference in the number of *WUS*-positive cells was taken into account, the RT-qPCR data indicated that individual cells in the *clv3* mutant expressed ∼22 times more *WUS*. In contrast, the amount of *WUS* per cell was not significantly changed in the *er erl1 erl2* mutant (Table 1). This result indicates that the function of CLV3 is to regulate the levels of *WUS* in cells of the central zone. On the other hand, ERfs restrict the *WUS* expression domain in the SAM periphery but do not control the cellular levels of *WUS* in the central zone. In addition, we observed a considerable variance in the number of *WUS*-positive cells in individual meristems of both mutants (Fig. 5I), suggesting that both CLV3 and ERfs are necessary for the SAM size stability.

The *clv3* mutant used (*clv3-9*) has a point mutation that results in a premature stop codon (W62STOP), but it still produces *CLV3* mRNA. Compared to the wild type, there were ∼9.7 and 3.5 times more *CLV3*-expressing cells in the *clv3* mutant and *er erl1 erl2* mutant, respectively (Fig. 5J). Surprisingly, the dramatic ∼22-fold increase in *WUS* in the *clv3* mutant led only to a relatively modest ∼2.1-fold increase in *CLV3* (Table 1). One possibility is that the premature stop codon decreases *CLV3* mRNA stability. However, it has previously been proposed that at high concentrations, WUS can inhibit *CLV3* expression (Perales et al., 2016). Whereas individual meristematic cells in the *er erl1 erl2* mutant did not have increased *WUS* expression, they accumulated approximately five times more *CLV3* (Table 1), suggesting that ERfs regulate *CLV3* expression in individual cells independently of *WUS*.

Next, we investigated whether, in *clv3* and *er erl1 erl2* mutants, there was a comparable increase in the number of cells expressing *WUS* and *CLV3*. In the wild type, there were 1.9 times more cells

Development (2024) 151, dev202870. doi:10.1242/dev.202870

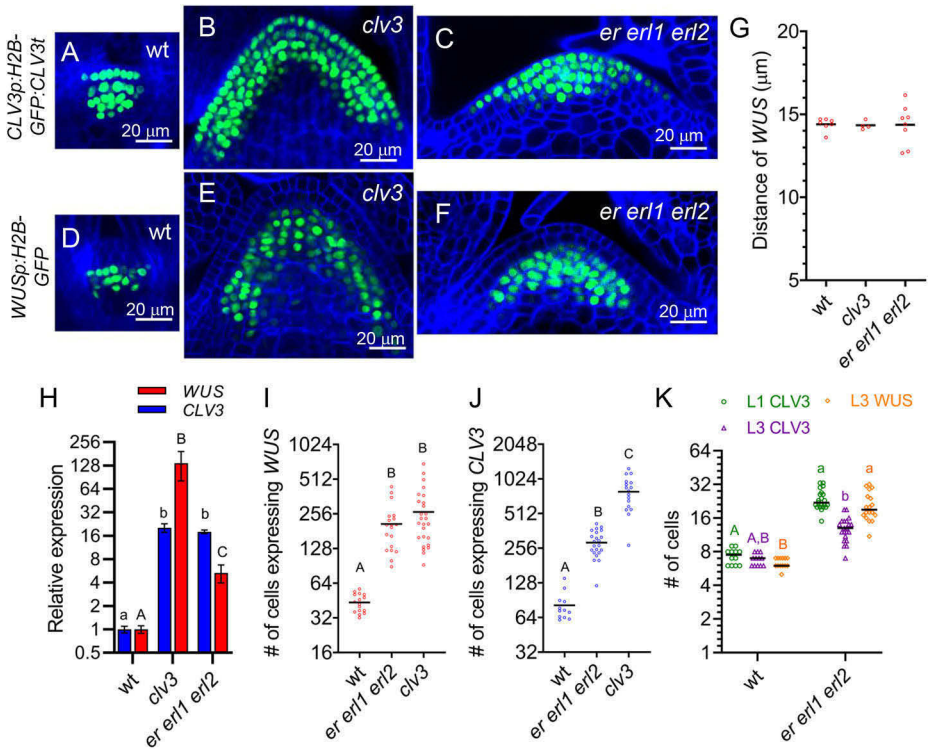

Fig. 5. CLV3 regulates the level of *WUS* expression but not its apical-basal pattern. (A-F) Confocal images of the SAM in 3DPG seedlings of the indicated genotypes (wt, wild type) expressing a promoter reporter construct for (A-C) *CLV3* (*CLV3p:H2B-GFP:CLV3t*; green) or (D-F) *WUS* (*WUSp:H2B-GFP*; green). The cell walls were stained with SR2200 (blue). All images are shown at the same magnification. (G) The distance of the *WUS* domain from the top of the SAM in 3DPG seedlings of the indicated genotypes, measured using the H2B-GFP reporter as shown in D-F. *n*=4-8. (H) RT-qPCR of *CLV3* and *WUS* in 3DPG seedlings of the indicated genotypes. *n*=15. (I,J) The number of cells expressing (I) *WUS* or (J) *CLV3* in 3DPG seedlings of the indicated genotypes, as assessed using the promoter reporters shown in A-F. *WUS*, *n*=16-26; *CLV3*, *n*=12-22. (K) The number of cells expressing *WUS* or *CLV3* in the L1 and L3 layers of the SAM of wild-type and *er erl1 erl2* seedlings, determined as described in I and J. *n*=12-21. Bars in G and I-K indicate the mean. Data in H are presented as the mean±s.d. For H-K, statistical differences were detected using a one-way ANOVA followed by a Tukey post-hoc test with $P<0.05$; letters denote statistically significance differences, with no statistically significant difference between groups marked by the same upper- or lower-case letter. In I-K, horizontal lines represent the mean and points represent individual seedlings.

expressing *CLV3* than cells expressing *WUS* (Table 1). This is consistent with the fact that *CLV3* is expressed in almost all *WUS*-expressing cells plus tunica cells. In the *clv3* mutant, the ratio of *CLV3* cells to *WUS* cells increased from 1.9 to 3.0 due to faster cell proliferation of the tunica cells. This proliferation leads to the convex shape of the *clv3* SAM. We were surprised that in the *er erl1 erl2* mutant, the ratio of *CLV3* cells to *WUS* cells decreased from 1.9 to 1.4. To understand the cause of this decrease, the expression of both genes was compared in individual cell layers of the wild type and the *er erl1 erl2* mutant (Fig. 5K). In the mutant, *CLV3* expression expanded very broadly in the L1 layer. However, it did not spread as widely in the internal tissues as *WUS* expression. This finding has several implications. First, it suggests a complex tissue-specific pattern in which *CLV3 e*xpression is regulated and that ERf signaling plays an especially strong role in the inhibition of *CLV3* expression in the L1 layer. An additional mechanism might restrict *CLV3* expression in the internal tissues of the meristem periphery. Second, uneven expansion of *CLV3* and *WUS* domains in the *er erl1erl2* mutant indicates that the changes in their expression are not due to the overall expansion of the central zone but are due to a particular mechanism by which ERfs regulate them.

A mechanistic model for 3D expression patterning in the SAM

Previous mathematical models for apical-basal patterning of gene expression in the SAM have either assumed or produced antiparallel gradients of *WUS* and *CLV3* expression with minimal overlap (Chickarmane et al., 2012; Hohm et al., 2010; Liu et al., 2020), which contradicts our 3D high-resolution imaging data (Fig. 5A-F;

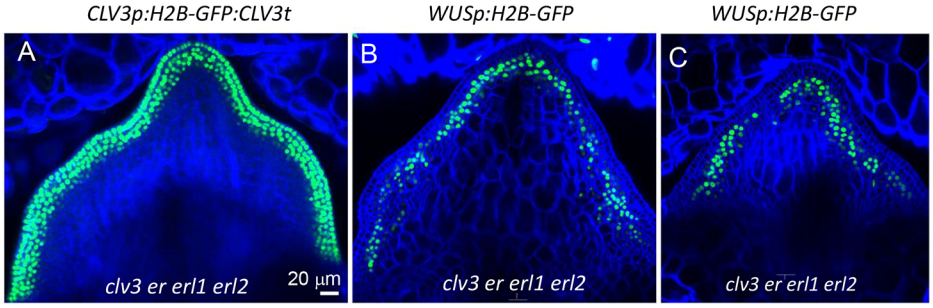

Fig. 6. In the *clv3 er erl1 erl2* mutant, cells that express *WUS* also express *CLV3*. (A-C) Representative confocal images of the SAM region of 3DPG *clv3 er erl1 erl2* seedlings transformed with a promoter reporter construct for either (A) *CLV3* (*CLV3p:H2B-GFP:CLV3t*; green) or (B,C) *WUS* (*WUSp:H2B-GFP*; green). All images are shown at the same magnification. The cell walls were stained with SR2200 (blue). Images are representative of ten seedlings for A and 20 for B and C.

Development (2024) 151, dev202870. doi:10.1242/dev.202870

Table 1. Comparison of *CLV3* and *WUS* expression

	Number of cells expressing *WUS*	Change in *WUS* expression/cell	Number of cells expressing *CLV3*	Change in *CLV3* expression/cell	Ratio of *CLV3* cells/*WUS* cells
WT	43.5±8.0	1×	81.7±23.9	1×	1.9×
clv3	265.8±151.3	22×	791.7±258.3	2.1×	3.0×
er erl1 erl2	208.8±97.0	1.1×	286.4±73.7	5.1×	1.4×

The number of cells with *WUS* or *CLV3* expression was determined using confocal images as shown in Fig. 5A-F. The changes in gene expression per cell were determined by dividing the fold increase in expression as determined by the RT-qPCR analysis in Fig. 5H by the fold change of the number of nuclei expressing the gene.

Movies 1-3). To test whether our current understanding of the regulatory network involving WUS, CLV3 and ERf signaling is sufficient to explain the up-to-date expression data, we built a 3D mathematical model that describes both the steady-state geometry of the SAM in terms of cell location and the expression regulation of *WUS* and *CLV3*. In this reaction-diffusion model, cells in the SAM were represented as 326 points in a 3D half dome. For gene regulation that occurs in cells, we considered the canonical negative feedback loop between WUS and CLV3 (Brand et al., 2000); the negative regulation of both *WUS* and *CLV3* by EPFLs, whose expression zones were restricted to the peripheral areas of the SAM (Kosentka et al., 2019; Zhang et al., 2021); and the negative regulation of *CLV3* by HAM (HAIRY MERISTEM protein family) signal from the meristem rib (Fig. 7A) (Han et al., 2020b). For WUS and CLV3, mRNA and protein levels were modeled separately. The model also considered movements of WUS, CLV3 and EPFLs between neighboring cells. Finally, we considered the inhibition of *CLV3* by high concentrations of WUS (Perales et al., 2016) (Fig. 7A, dashed line). We restricted the *WUS* expression to L3 and lower layers and the HAM signal to the 6th layer from the epidermis and below to account for other spatial factors (e.g. cytokinin receptor) not described in the model (Fig. 7B).

We fitted the model to our high-resolution experimental data using biologically plausible parameter values. The model reproduced the *CLV3* expression region encompassing the *WUS* expression region under the wild-type condition (Fig. 7C). This substantial overlap was also observed with the *er erl1 erl2* mutant (*erf* mutant; the removal of EPFL signal) and the *clv3* mutant (note that in the latter case, the *CLV3* mRNA is produced but nonfunctional). In addition to the *CLV3*-*WUS* overlap, the absence of EPFL signal resulted in an expansion of the *WUS* expression region, but the level of expression in *WUS* mRNA-containing cells was unchanged (Fig. 7D). In contrast, the absence of functional CLV3 gave rise to both expansion of expression region and single-cell upregulation of *WUS* (Fig. 7E). The expression of *CLV3* in both mutants was expanded in the SAM, but its single-cell upregulation was much less prominent compared to that of *WUS* (Fig. 7D,E).

We found that the loss of *CLV3* inhibition by high concentration of WUS resulted in both expansion and single-cell upregulation of CLV3 expression (compare Fig. 7F and C). We next asked whether the inhibition of both *CLV3* and *WUS* by EPFLs is required for correct SAM patterning. The removal of *CLV3* inhibition by EPFLs resulted in upregulation of *CLV3* in single cells and expansion of *CLV3* expression (Fig. 7G), whereas the removal of *WUS* inhibition by EPFLs resulted in expansion of the expression regions of both *CLV3* and *WUS* (Fig. 7H). The slight decrease in *WUS* expression was due to *CLV3* upregulation (Fig. S4). This suggests that the two regulations by EPFLs are required for SAM patterning. Taken together, our experimentally inspired 3D model reproduced both key single-cell expression changes upon perturbations and distributions of gene expressions that were not captured by previous models simultaneously (Zhou et al., 2018; Liu et al., 2020). The model also suggests new mutant phenotypes that can be tested in future experiments.

DISCUSSION

The role of ERf/EPFL signaling in regulation of *CLV3* and *WUS* expression

ERfs are important negative regulators of SAM size, functioning through suppression of *CLV3* and *WUS* expression (Chen et al., 2013; Uchida et al., 2013, 2012b; Mandel et al., 2014; Zhang et al., 2021). The analysis of transcriptome changes after brief activation of ERf signaling confirmed that these two genes are the core targets of the pathway in the SAM. A mechanistic model for 3D expression patterning in the SAM indicated that regulation of both genes is necessary for the correct SAM patterning. The three ERfs redundantly control the width of the vegetative SAM and are particularly important during embryogenesis when the meristematic domain is defined (Chen et al., 2013; Uchida et al., 2012b). This is in contrast to CLV3 signaling, which controls both the width and the height of the SAM and functions in maintaining the meristem at a relatively constant size throughout the life of a plant (Clark et al., 1995). Consistent with their different roles in SAM establishment and maintenance, ERfs and CLV3 play distinct roles in the regulation of *WUS*. ERfs regulate the width of the *WUS* domain, suppressing its expression in the periphery of the SAM. Thus, ERf signaling contributes to the patterning of the SAM, defining different zones. In contrast, CLV3 regulates the cellular concentration of *WUS* in the central zone, defining its size.

The second function of ERfs is to reduce CLV3 cellular levels and prevent its expression in the periphery of the SAM, especially the L1 layer. ERfs regulate *CLV3* independently of *WUS*, since in the central zone of the *er erl1 erl2* mutant, the *CLV3* cellular levels increase without an increase of *WUS* cellular levels, and knockout of ERf signaling in the *wus* background promotes *CLV3* expression (Kimura et al., 2018). In early land plants, CLV regulates auxin and cytokinin signaling and does it independently of WUS homeobox-containing (WOX) genes (Fouracre and Harrison, 2022), as WUS-lineage WOX genes first appeared only in ferns (Nardmann and Werr, 2012). In liverwort, *Marchantia polymorpha*, CLAVATA signaling regulates meristematic cells independently of its only WOX gene (Hirakawa et al., 2020). We speculate that in angiosperms, CLV3 signaling might have other targets besides WUS, and suppression of *CLV3* by ERfs might be related to these other functions.

The activity of ERfs is regulated by small extracellular cysteine-rich proteins from the EPF/EPFL family. In *Arabidopsis*, this family consists of eleven genes that form four clades (Takata et al., 2013). The function of two clades is linked with the formation of stomata (Richardson and Torii, 2013). The other two clades regulate the SAM (Kosentka et al., 2019). There are differences in the expression and overall function of these two last clades. One clade, consisting of EPFL4, EPFL5 and EPFL6 (EPFL4/5/6), promotes elongation of aboveground organs. EPFL4 and EPFL6 are expressed in the endodermis and regulate the elongation of internodes and pedicels

Development (2024) 151, dev202870. doi:10.1242/dev.202870

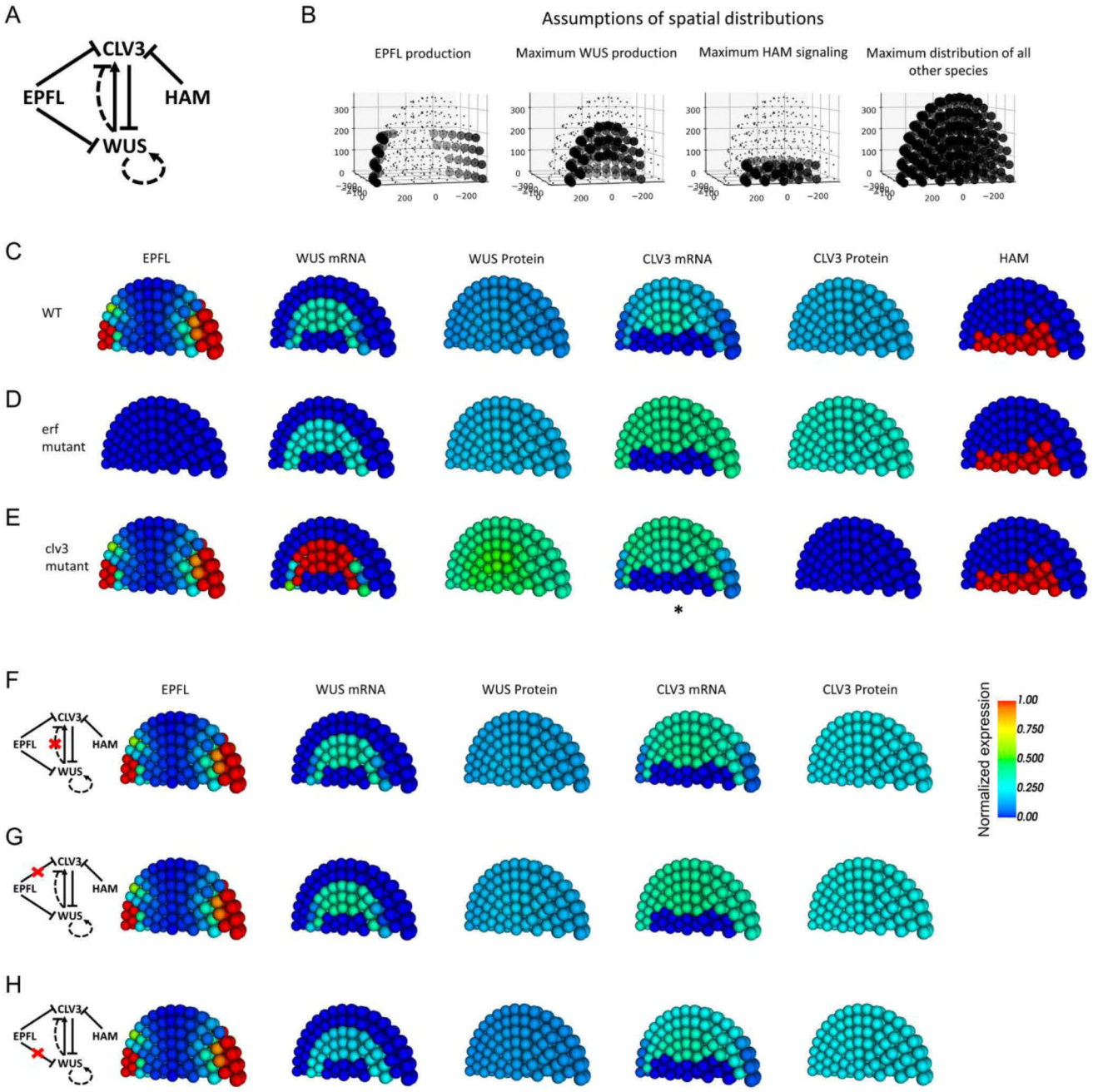

Fig. 7. A mathematical model of SAM patterning. (A) General gene regulatory network describing transcriptional regulation in the SAM. For *CLV3* and *WUS*, both mRNA and protein are explicitly described, whereas only proteins were explicitly described for EPFLs and HAM. (B) Assumptions of maximum spatial distributions of regulatory factors in the absence of the regulations shown in A. Dots show the positions of simulated cells. Small dots indicate the absence of the factor from the regulatory network in A. Each length unit represents approximately 0.025 µm. (C-E) Model simulations under experimental conditions included in this study. The colors of the balls, which represent cells within the SAM, show normalized expression levels of the indicated factors (see Materials and Methods). *CLV3* mRNA in the *clv3* mutant (asterisk) is nonfunctional and is not translated. Because ERF mutants cannot perceive EPFL signals, in D the loss of ERF function (*erf* mutants) is represented as loss of EPFL expression. (F-H) Additional model conditions for predictions of the roles of specific transcriptional regulations. The specific transcriptional regulation perturbed in each panel is indicated by a red X.

(Abrash et al., 2011; Uchida et al., 2012a). All three genes redundantly promote the elongation of stamen filaments (He et al., 2023; Negoro et al., 2023; Huang et al., 2014). Another clade consists of EPFL1, EPFL2 and EPFL3 (EPFL1/2/3). EPFL2 regulates ovule initiation, elongation of leaf teeth and growth of cotyledons, and it is often expressed in organ boundaries (Tameshige et al., 2016; Kawamoto et al., 2020; Fujihara et al., 2021). EPFL4/5/6 and EPFL1/2/3 differ not only in function but also in structure. All EPF/EPFLs are made of a loop and a scaffold (Ohki et al., 2011). The loop structure is important for ligand function and might define whether it is an agonist or antagonist. EPFL9 is an antagonist; it competes with EPF2 for the same receptors but does not activate the downstream mitogen-activated protein kinase cascade (Lee et al., 2015). Swapping the loops between EPF2 and EPFL9 reverses their function (Ohki et al., 2011). The sequence and length of loops differ significantly between EPFL1/2/3 and EPFL4/5/6 clades.

Development (2024) 151, dev202870. doi:10.1242/dev.202870

EPFL1, EPFL2, EPFL4 and EPFL6 redundantly regulate SAM width, leaf initiation and internode elongation (Kosentka et al., 2019). But do they regulate the same set of genes? Previously, we have demonstrated that EPFL4 and EPFL6 inhibit the expression of *WUS* and *CLV3* (Zhang et al., 2021). Our current work shows that EPFL1 and EPFL2 also regulate the expression of these two genes. In summary, although the two clades of EPFL ligands differ structurally, their function in the SAM is very similar.

Previously, we have observed that whereas the SAM of the *clv3 er erl1 erl2* mutant forms very few organs, the SAM of the *clv3 epfl1,2,4,6* mutant forms some leaves and flowers (Zhang et al., 2021). Our current comparison of *WUS* and *CLV3* expression in *er erl1 erl2* and *epfl1,2,4,6* mutants detected some small but statistically significant differences. This finding suggests that either ERfs regulate the SAM in a ligand-independent manner or other EPFLs also regulate the SAM structure.

ERf/EPFL signaling does not designate cells for leaf primordia but promotes primordia outgrowth

ERf signaling promotes the initiation of cotyledons and leaves and regulates phyllotaxis (Chen et al., 2013; DeGennaro et al., 2022). The hormone auxin induces initiation of aboveground organs. However, in the absence of ERf signaling, auxin cannot initiate leaves and cotyledons efficiently (DeGennaro et al., 2022). Previously, we have proposed that auxin and ERfs have common downstream targets (DeGennaro et al., 2022). In *Arabidopsis*, two AP2/ERF transcription factors, *DRN* and *DRNL,* promote cotyledon and leaf initiation (Chandler et al., 2007). During organogenesis, *DRNL* is expressed in incipient organ primordia before the formation of auxin response maxima, and it functions synergistically with auxin and PID (Chandler et al., 2011). DRNL in complex with transcription factor MONOPTEROS (MP) inhibits cytokinin accumulation in forming primordia (Dai et al., 2023). Our RNAseq data indicated that in the absence of CHX, a brief activation of ERf signaling promotes *DRN* and *DRNL* expression; however, in the presence of CHX, it downregulates *DRN* and *DRNL* expression. To understand the role of ERf signaling in the regulation of these two genes, we analyzed their expression in the SAM. This analysis indicated that *DRN* and *DRNL* are expressed more broadly in the *epfl1,2,4,6* mutant than in the wild type, which is consistent with the downregulation of *DRN* and *DRNL* by EPFL6 in the presence of CHX. Overall, these data indicate that cells designated to become leaf primordia are specified, but some other requirements for leaf primordia outgrowth still must be met.

Transcriptomic analysis identified the MEI2 family of RNA-binding proteins as additional putative targets. Nine MEI2 family genes in *Arabidopsis* form two clades (Anderson et al., 2004). We found that EPFL6 inhibits the expression of three genes belonging to the same clade: *MCT1*, *MCT2* and *TEL2*. Based on *in situ* hybridization, all three of these genes are expressed in the central zone of the SAM (Anderson et al., 2004; Yadav et al., 2009). In maize, rice and moss, these genes inhibit leaf initiation and control phyllotaxy (Veit et al., 1998; Xiong et al., 2006; Kawakatsu et al., 2006; Vivancos et al., 2012), but their meristematic function in *Arabidopsis* is unknown. It is tempting to speculate that ERfs regulate organogenesis by inhibiting MEI2 family gene expression. However, analysis of the function of these genes function in *Arabidopsis* is necessary before any definitive conclusion can be made.

CLV3 controls *WUS* cellular levels but not the apical-basal position of its expression domain

In *Arabidopsis*, the WUS-CLV3 negative feedback loop is central to the stability of the SAM size (Han et al., 2020a). WUS promotes the identity and proliferation of stem cells. CLV3 inhibits the expression of *WUS* to prevent stem cell overproliferation. Because *WUS* positively regulates *CLV3* expression, CLV3 signaling can decrease *WUS* expression only to a certain extent and can never completely shut it down. The prevailing model asserts that the function of CLV3 is not only to regulate cellular levels of *WUS* but also to position the *WUS* domain in the deeper tissues of the SAM. This model was proposed during early investigations of the CLV3 and WUS feedback loop. Comparisons of *WUS* expression in the wild type and the *clv3* mutant by *in situ* hybridization have been interpreted as showing that *WUS* is expressed in deep layers of the SAM and that WUS expression moves upward directly under the L2 cell layer when *CLV3* is absent (Schoof et al., 2000; Brand et al., 2000). However, multiple published *in situ* hybridization images show that in the wild type, *WUS* is expressed directly under the L2 layer in both the vegetative and inflorescence SAM (Luo et al., 2018; Lenhard and Laux, 2003; Mayer et al., 1998; Hu et al., 2018). In addition, the original manuscript by Schoof and colleagues states that in embryos, *WUS* is expressed directly under the L2 layer in the wild type, and its expression domain does not move upward in the *clv3* mutant (Schoof et al., 2000). An examination of *in situ* hybridization images of *WUS* expression in the manuscript by Brand and colleagues shows *WUS* expression directly under the L2 layer in the wild type (Brand et al., 2000). In wild-type meristems, the presence of *WUS* mRNA directly under the L2 layer has been observed for *pWUS:GFP:WUS*, *pWUS:WUSlinker-GFP* and *pWUS:2×Venus-NLS:tWUS* constructs (Yadav et al., 2011; Daum et al., 2014; Gruel et al., 2016; Wenzl and Lohmann, 2023). Despite all this evidence, the assumption that CLV3 regulates *WUS* expression along the apical-basal axis has not been explicitly challenged. All recent reviews show only a partial overlap of *CLV3* and *WUS* expression, with the majority of *WUS* expression occurring in the cells that do not express *CLV3* (Truskina and Vernoux, 2018; Uchida and Torii, 2019; Fuchs and Lohmann, 2020; Han et al., 2020a; Hirakawa, 2021; Lopes et al., 2021; Shimotohno, 2022; Ince and Sugimoto, 2023).

The correct detection of *WUS* expression in *in situ* hybridization images depends on precise vertical sectioning exactly through the center of the SAM. If the section is made at an oblique angle, the *WUS* expression will be perceived to be deeper than it is. We analyzed *WUS* expression using the *WUSp:H2B-GFP* promoter reporter construct. This construct contains a 4.5 kb regulatory sequence that has been used previously and that includes all regulatory elements necessary for expression in the SAM (Yadav et al., 2009; Bäurle and Laux, 2005; Zhang et al., 2017). When we examined two-dimensional images, we realized that they provide an inconsistent pattern of *WUS* expression and are challenging to interpret. However, analysis of *z*-stacks firmly placed *WUS* expression in the third and fourth cell layers of the SAM in the wild type and in any mutant that we observed. There was no shift of *WUS* expression apically in the *clv3* mutant. If there was any expansion of *WUS* expression along the apical-basal axis, it was basally into the fifth layer in some *clv3* mutant and *epfl* mutant seedlings. The expression of *WUS* is induced by cytokinins, which are produced in the L1 layer of the SAM but are perceived only underneath the tunica (Lindsay et al., 2006; Gordon et al., 2009; Chickarmane et al., 2012). Diffusion of cytokinins from the L1 layer tethers *WUS* expression to a specific distance from the apex; there is no apparent need for additional regulation. Our data indicate that CLV3 does not define the *WUS* expression domain but controls the concentration of *WUS* in the central zone.

Based on published *in situ* hybridization images, expression of *CLV3* varies and can be detected in either three or four top layers of

Development (2024) 151, dev202870. doi:10.1242/dev.202870

the SAM (Brand et al., 2000; Fletcher et al., 1999; Lenhard and Laux, 2003; Reddy and Meyerowitz, 2005). This inconsistency could be due to differences in the SAM sectioning (through the middle or at an angle); differences between vegetative, inflorescence and floral meristems; or variable growth conditions. Recent findings suggest that the depth of *CLV3* expression is regulated by temperature, with higher temperatures inhibiting *CLV3* expression in the deeper tissues (Wenzl and Lohmann, 2023). Our data indicate that in the vegetative SAM at 21°C, *CLV3* is expressed in the four top cell layers in the wild type and in the *clv3*, *er erl1 erl2*, *epfl* and *clv3 er erl1 erl2* mutants, and that *CLV3* expression strongly overlaps with *WUS*. Thus, in the vegetative SAM, *CLV3* should regulate *WUS* cellular levels through autocrine signaling, which is typical for CLE peptides (Narasimhan and Simon, 2022). Modeling predicted that the overlap of *CLV3* and *WUS* expression removes the necessity for HAM influence close to the epidermis in the SAM. Consistently, we observed that *CLV3* expression in the L1 layer and deeper tissues is controlled differently. Further research on the mechanisms controlling *CLV3* expression should provide deeper insights into the molecular processes that oversee the size of the SAM and impact the overall plant architecture.

MATERIALS AND METHODS

Plant materials and growth conditions

The *Arabidopsis thaliana* ecotype Columbia was used as the wild type. The following mutants have been described previously: *er-105 erl1-2 erl2-1* (*er erl1 erl2*; Shpak et al., 2004); *epfl1-1 epfl2-1* (abbreviated here as *epfl1,2)*, *cll2-1 chal-2/epfl4 epfl6* (abbreviated here as *epfl4,6)*, *epfl2,4,6* and *epfl1,2,4,6* (Kosentka et al., 2019); *clv3-9* (Nimchuk et al., 2015); and *clv3 epfl1,2,4,6* (Zhang et al., 2021). All mutants are in the Columbia background. Seedlings were grown on modified Murashige and Skoog medium (Research Products International) plates supplemented with 1% (w/v) sucrose. Plates were stratified for 2 days at 4°C and then moved to a growth room with the following conditions: 18 h light/6 h dark cycle and 21°C. The generation of the wild-type plants expressing *WUS* promoter reporter (*WUSp:H2B-GFP:35St*; pESH746) and *CLV3* promoter reporter (*CLV3p:H2B-GFP:CLV3t*; pESH747) constructs was described previously (Zhang et al., 2021). These constructs were transformed into *clv3*; *epfl1,2*; *epfl4,6*; *epfl1/+,2,4,6*; and *clv3 er erl1 erl2* plants.

The *DRN* promoter reporter construct (DRNp:H2B-eGFP:DRNterm) was generated by fusing the 4.86 kb sequence upstream of the *DRN* start codon with sequence encoding H2B-eGFP followed by a 1.38 kb sequence downstream of the *DRN* stop codon (Kirch et al., 2003; Luo et al., 2018). The H2B-eGFP sequence was fused to the downstream sequence using overlapping PCR and inserted into the binary vector pPZP222 (Hajdukiewicz et al., 1994) between BamHI and SalI sites. The template for amplifying the H2B-EGFP sequence was a plasmid from the Z. Nimchuk lab (UNC Chapel Hill, USA). The H2B-eGFP:DRNterm plasmid was used as a vector to introduce the 4.86 kb *DRN* promoter sequence using BamHI, and the plasmid was named pAMO102b. The *DRNL* promoter reporter construct (DRNLp:H2B-eGFP:35sT) was generated by fusing the 4.3 kb sequence upstream of the *DRNL* start codon to H2B-eGFP:35sTerm (Luo et al., 2018). Using overlapping PCR, H2B-eGFP was linked to the CaMV 35S terminator and inserted into the binary vector pPZP222 between BamHI and SalI sites. This plasmid was used as a vector to introduce the 4.3 kb *DRNL* promoter between KpnI and BamHI sites, and the construct was named pAMP109. Both constructs were confirmed by Sanger sequencing.

The following construct was generated to produce dexamethasone–inducible EPFL2 expressed in its endogenous domain (Fig. S2). The 2.58 kb promoter of *EPFL2* was amplified using pPZK412 (Kosentka et al., 2019) and fused with GR-LhG4:T35S amplified from pBIN-LhGR-N (Samalova et al., 2005) via overlapping PCR. This DNA fragment was introduced into the binary vector pPZP222 between KpnI and SbfI sites, and the plasmid was named pAMO112. The next step involved eight PCR reactions. PCR1 amplified H2B-GFP:35S terminator (T_{35S}). PCR2 amplified the omega translational enhancer (Ω) and 35S minimal promoter (35S Min) using plasmid pH-TOP (Samalova et al., 2005) as a template. PCR1 and PCR2 products were overlapped to generate a PCR3 fragment. PCR4 used pH-TOP as a template to generate a fragment containing pPOP6 followed by 35S Min and Ω. PCR5 amplified the EPFL2 coding sequence with introns using the pPZK412 vector as a template. PCR6 amplified the NOS terminator (T_{NOS}) using pBIN-LhGR-N as a template. PCR7 was an overlapping PCR that fused DNA fragments created by PCR4, PCR5 and PCR6. Finally, PCR8 was an overlapping PCR that fused the PCR3 and PCR7 DNA fragments. It generated a DNA fragment containing T_{35s}:H2B-GFP: Ω:35SMin:pOp6:35SMin: Ω:gEPFL2: T_{NOS}. The DNA segment generated by PCR8 was inserted into the SbfI site of pAMO112. Orientation was confirmed via restriction digest and Sanger sequencing. The sequencing identified additional SbfI sites between the two T_{35S}. The final construct was named pAMO113 and contained: proEPFL2:GR-LhG4: T_{35S}___T_{35S}:H2B-GFP:Ω:35sMin_pOp6_35sMin:Ω:gEPFL2:T_{NOS}.

The generated constructs were transformed into an *Agrobacterium tumefaciens* strain GV3101/pMP90 by electroporation and introduced into wild-type (Columbia ecotype); *epfl1,2*; and *epfl1/+,2,4,6* plants by the floral dip method (Clough and Bent, 1998).

To induce EPFL2, an *epfl1,2,4,6* mutant expressing pAMO113 was grown on modified Murashige and Skoog medium (MS-0) plates for 5 days (3DPG). Then, 15 seedlings per biological replicate were transferred to 2 ml of liquid MS-0 containing 10 µM DEX (Thermo Scientific Chemicals) or an equivalent amount of DMSO (mock treatment). The 50 mM stock solution of DEX was prepared using DMSO. 24-well culture plates with the samples were kept on a rocker in a growth room for 7 h, and then seedlings were preserved in liquid nitrogen.

Due to the infertility of the *epfl1,2,4,6* mutant, we isolated it from the progeny of *epfl1/+,2,4,6* plants. A small piece of root was cut from a seedling and placed into the PCR mix. PCR was performed using the Phire Plant Direct PCR Master Mix kit (Thermo Fisher Scientific). The rest of the seedling was preserved in 4% paraformaldehyde for microscopy. A three-primer PCR reaction with EPFL1.74, EPFL1.436.rev and 3dspm (Table S2) was performed to genotype for *epfl1*. The mutant band was ∼200 bp, and the wild-type band 387 bp.

RNAseq library construction, sequencing and analysis of differential gene expression

For the RNAseq sample collection, seedlings were grown as described previously (Zhang et al., 2021). In brief, the *clv3 epfl1,2,4,6* seedlings were grown on modified Murashige and Skoog medium plates for 5 days (3DPG). Four treatment conditions were used: mock, 10 µM EPFL6, 10 µM cycloheximide (CHX; Alfa Aesar), and a combination of 10 µM EPFL6 and 10 µM cycloheximide. Purification of the EPFL6 peptide was described previously (Lin et al., 2017). EPLF6 peptides were diluted in 10 mM Bis-Tris and 100 nM NaCl, pH 6.0 (treatment buffer). For treatment, 10 seedlings per biological replicate were transferred into 1 ml of liquid Murashige and Skoog medium. Seedlings in liquid medium were treated with 8.7 µl of the 1.15 mM EPFL6 solution or for mock with an equal volume of the treatment buffer. For CHX treatments, seedlings in a liquid medium were pretreated with 10 µM CHX for 10 min before EPFL6 or the mock treatment was added. The aboveground portion of the seedlings was collected 3 h after adding EPFL6 or the mock treatment buffer and flash frozen in liquid nitrogen. Three biological replicates were performed for each treatment. Total RNA was isolated using the Spectrum Plant RNA Isolation Kit (Sigma-Aldrich).

RNA quality was measured using 4200 TapeStation (Agilent); all samples had an RNA integrity number (RIN) score greater than 7.5. Paired-end cDNA libraries were constructed using the TruSeq mRNA kit from Illumina. The libraries were sequenced on a NovaSeq S4 flow cell in paired-end mode and with 150 base pair reads at the Oklahoma Medical Research Foundation. Raw read quality was assessed with FastQC v0.11.5 (Babraham Bioinformatics). Raw reads were aligned to the TAIR10.1 genome and Araport11 annotation (TAIR genome and Araport11 citation) using STAR-2.7.6a (Dobin et al., 2013), with default parameters except for the following: - alignIntronMax 1000. Mapping quality was assessed with RSeQC v4.0.0 (Wang et al., 2012). Reads were counted using subread featureCounts v2.0.1

Development (2024) 151, dev202870. doi:10.1242/dev.202870

(Liao et al., 2013) in paired-end mode. Reads were imported into R (v3.6.3). Genes not expressed in all three replicates of at least one sample were removed. Samples were inspected for batch effect by PCA, and no batch effect was found. The filtered reads were then normalized, and differential gene expression was assessed using DESeq2 v1.26.0 (Love et al., 2014) using a two-factorial design. The resulting *P*-values were corrected for multiple comparisons using FDR, and the resulting $\log_2$ fold changes were shrunk using ashr2.2 (Stephens, 2017).

RT-qPCR analysis

Total RNA was isolated from the tissues of 3DPG seedlings using the Spectrum Plant RNA Isolation Kit (Sigma-Aldrich). The RNA was treated with RNase-free RQ1 DNase (Promega). First-strand complementary cDNA was synthesized with LunaScript RT SuperMix Kits (New England Biolabs). Quantitative PCR was performed with a CFX96 Touch Real-Time PCR Detection System (Bio-Rad) using SsoAdvanced Universal SYBR Green Supermix (Bio-Rad). Each experiment contained three technical replicates of three biological replicates. Cycling conditions were as follows: 30 s at 95°C; then 40 repeats of 10 s at 95°C, 10 s at 52°C for *ACTIN2*, 55°C for *WUS* and *GFP*, 53°C for *CLV3*, 56.7°C for *MCT1*, 50°C for *MCT2* and *EPFL2*, and 56.1°C for TEL2, and 15 s at 68°C, followed by the melt-curve analysis. For *AtFEA3*, two-step PCR was performed. Cycling conditions were as follows: 30 s at 95°C; then 40 repeats of 10 s at 95°C, 30 s at 68°C, followed by the melt-curve analysis. qPCR for *ACTIN2*, *CLV3*, *EPFL2* and *GFP* was performed in 10 µl with 4 µl of 10× diluted cDNA, whereas *WUS*, *AtFEA3*, *MCT1*, *MCT2* and *TEL2* were performed in 20 µl with 8 µl of 10× diluted cDNA reaction. All primers used in this study are shown in Table S2. The fold difference in gene expression was calculated using relative quantification by the $2^{-\Delta\Delta CT}$ algorithm (Livak and Schmittgen, 2001) *ACTIN2* was used as an internal control.

Microscopy

For microscopy, we used the T3 or T4 generations of transgenic plants that were homozygous for the insert, except when the *WUS* reporter was analyzed in T2 *epfl1,2* and *epfl4,6* seedlings. 3-day-old seedlings were fixed with 4% paraformaldehyde for 1.5 h. The fixed samples were washed three times for 5 min in phosphate buffer (PBS) and cleared with ClearSee (Kurihara et al., 2015) for 3 days at room temperature on a rocker. The cell wall was stained with Renaissance 2200 [0.1% (v/v) in ClearSee] (Musielak et al., 2015) for 1-2 days. For better imaging, one cotyledon was removed under a stereo microscope. A Leica SP8 confocal microscope (Leica Microsystems, Wetzlar, Germany) with 40×/1.10 water objective was used at the Advanced Microscopy and Imaging Center, University of Tennessee, Knoxville, TN, USA. An argon laser with 488 nm emission was used for the excitation of EGFP, and images were collected using a HyD 'Hybrid' Super Sensitivity SP Detector with the emission range of 493-550 nm. SCRI Renaissance 2200 (SR2200) dye was excited with a diode 405 nm 'UV' laser, and images were collected by using PMT SP Detector with the emission 415-470 nm. EGFP and SR2200 fluorescence emission was collected with HyD 'Hybrid' Super Sensitivity SP Detector (Leica Microsystems) and PMT SP Detector (Leica Microsystems). *Z*-stacks were created via sequential line scanning. Quantitative image measurements were performed using the Fiji image processing software (Schindelin et al., 2012). Two-dimensional slices from the center of the SAM were chosen based on analysis of *z*-stacks to determine the width and height of reporter expression. The spot detection tool of IMARIS software (Oxford Instruments) was used to calculate the number of cells in Fig. 5I-K and Table 1. Nuclei were detected on the basis of EGFP signal, and estimated nuclei diameter values were used for background subtraction.

Construction of the mathematical model

We assumed that there is a two-fold symmetry of the SAM. We used 326 points in a quarter ball (half dome) with a radius of 400 length units to represent cells in half of the SAM. The number of cells was estimated from Chen et al. (2013). In the 3D cell network model, the EPFL ligands are synthesized in two peripheral regions represented by two 'corner' regions. We assumed that EPFLs diffuses broadly in the SAM and inhibit the expression of both *WUS* and *CLV3* through binding to their receptors, which were assumed to be always expressed in each cell (Kosentka et al., 2019; Zhang et al., 2021). Because CLV3 is a diffusive peptide, and WUS is a transcription factor capable of moving between cells (Daum et al., 2014; Lenhard and Laux, 2003; Yadav et al., 2011), we assumed that these molecules are diffusible in the model. Our model includes WUS-CLV3 negative feedback and its lateral regulator, the EPFLs. In addition, the model describes a HAIRY MERISTEM (HAM) signal that originates from the rib zone and inhibits *CLV3* expression in the organizing center (Zhou et al., 2018). The distribution of *HAM* expression is likely established by other signals not considered in the model (Han et al., 2020b). It has been shown that a high concentration of WUS can cause *CLV3* downregulation, forming a biphasic regulation of *CLV3* by WUS (Perales et al., 2016; Shimotohno and Scheres, 2019), and this regulation is described in our model. The model also includes a CLV3-independent positive feedback involving WUS. This feedback can be supported by a WUS-cytokinin mutual activation loop: it has previously been shown that cytokinin activates *WUS* expression (Gordon et al., 2009; Chickarmane et al., 2012; Wang et al., 2017), whereas WUS derepresses cytokinin signal by inhibiting type A *ARABIDOPSIS RESPONSE REGULATOR* (ARR) genes, which act as inhibitors of cytokinin (To et al., 2004; Leibfried et al., 2005; Shimotohno and Scheres, 2019). This positive feedback loop might also be supported by other factors (Yadav et al., 2013). Based on these assumptions, the dynamics of six interacting species representing concentrations of regulatory molecules are described with nonlinear ordinary differential equations (ODEs) in each cell (point) of the model (additional spatial constraints are shown in Fig. 7B):

$$\frac{dW_p}{dt} = k_w W_r - b_W W_p + D_W \Delta W_p$$

$$\frac{dC_p}{dt} = k_c C_r - b_C C_p + D_C \Delta C_p$$

$$\frac{dW_r}{dt} = k_{0WW} \frac{k_{0WL}}{1 + \left(\frac{L}{K_{WL}}\right)^{n_{WL}}} \frac{k_{0WC}}{1 + \left(\frac{C_p}{K_{WC}}\right)^{n_{WC}}} \left(a_{w0} + \frac{\left(\frac{W_p}{K_{WW}}\right)^{n_{WW}}}{1 + \left(\frac{W_p}{K_{WW}}\right)^{n_{WW}}} \right) - b_{W_r} W_r$$

$$\frac{dC_r}{dt} = \frac{g_c}{1 + \left(\frac{L}{K_{CL1}}\right)^{n_{CL1}}} \left(a_C + \frac{\left(\frac{W_p}{K_{CW2}}\right)^{n_{CW2}}}{\left(1 + \left(\frac{W_p}{K_{CW2}}\right)^{n_{CW2}}\right)\left(a_{pc} + \left(\frac{W_p - W_{pc}}{K_{CW3}}\right)^{n_{CW3}}\right)} \right) \frac{1}{1 + \left(\frac{H}{K_{CH1}}\right)^{n_{CH1}}} - b_{C_r} C_r$$

$$\frac{dL}{dt} = k_L - b_L L + D_L \Delta L$$

$$\frac{dH}{dt} = k_H - b_H H.$$

Here, state variables W_r, W_p, C_r, C_p, L and H represent the concentrations (or strengths) of *WUS* mRNA, WUS protein, *CLV3* mRNA, CLV3 protein, EPFLs and HAM, respectively. A full list of parameter descriptions and their numerical values is available in Table S3. In the ODEs, k_w is the production rate constant of WUS protein; b_W is the degradation rate constant of WUS protein; K_{WC} is the threshold of inhibition of *WUS* by *CLV3*. n_{WC} is the cooperativity of inhibition of *WUS* by *CLV3*; D_W is the rate constant of passive diffusion-like transport of molecule WUS protein; k_c is the production rate constant of CLV3 protein. b_C is the degradation rate constant of *CLV3* protein. D_C is the rate constant of passive diffusion-like transport of molecule CLV3 protein. k_{0WW} is the production rate constant of *WUS* mRNA. k_{0WL} is the proportion of *WUS* mRNA production rate controlled by EPFLs. K_{WL} is the threshold of WUS inhibition by EPFLs. n_{WL} represents the cooperativity of

Development (2024) 151, dev202870. doi:10.1242/dev.202870

regulation of WUS by EPFLs. k_{0WC} is the proportion of *WUS* mRNA production rate controlled by CLV3. K_{WW} is the activation threshold of WUS autoactivation. n_{WW} is the cooperativity of WUS self-regulation. b_{W_r} is the degradation rate constant of *WUS* mRNA. g_c is the production rate constant of *CLV3* mRNA. K_{CL1} is the threshold of CLV3 inhibition by EPFL. n_{CL1} is the cooperativity of regulation of CLV3 by EPFLs. K_{CW2} is the threshold of CLV3 activation by WUS. n_{CW2} is the cooperativity of regulation of CLV3 by WUS. a_{pc} is the constant representing the inversed strength of CLV3 inhibition by WUS. K_{CW3} is the threshold of CLV3 inhibition by WUS. n_{CW3} represents the cooperativity of negative regulation of CLV3 by WUS. K_{CH1} is the threshold of CLV3 activation by HAM. n_{CH1} represents the cooperativity of regulation of CLV3 by HAM. b_{C_r} is the degradation rate constant of *CLV3* mRNA. k_L is the production rate constant of EPFL. b_L is the degradation rate constant of EPFL protein. D_L is the passive diffusion rate constant of EPFL proteins. k_H is the production rate constant of HAM. b_H is the degradation rate constant of HAM protein; Δ is the Laplace operator describing gradients of concentrations, which govern passive diffusion-like transport; ΔW_p, ΔC_p, ΔL have a unit of concentration per unit area. D_W, D_C, D_L were adjusted by multiplying with a scaling factor l/l, where l represents the distance between the centers of the two cells (Delile et al., 2017); and neighboring cells are defined as cells that are located within a radius of 100 length units (~10 µm). We neglected the subcellular geometry of the cells, their contact areas and the influence of mechanics in this study (the effective contact area for WUS transport cannot be directly inferred from total contact area of plasma membrane). The movements of EPFLs, CLV3 and WUS are responsible for the intercellular communication in the model. We used a Hill function to describe nonlinearity in the gene regulation. Previous models of the SAM and other complex systems have used similar nonlinear functions (Fujita et al., 2011; Nikolaev et al., 2007; Ye et al., 2019; Gruel et al., 2018; Liu et al., 2020). a_C is a constant used to perturb the negative feedback regulation. a_{w0} is a constant used to perturb the auto-positive feedback regulation. Because the absolute concentrations of these molecules have not been measured experimentally, we used an arbitrary unit (a.u.) to describe concentration (or strength) of each molecule. We used a no-flux boundary condition for the model, as in other published SAM models (Zhou et al., 2018; Liu et al., 2020).

We fitted the parameters to known patterning phenotypes of the SAM under normal and genetically perturbed conditions. The *erf* mutant was represented by setting the EPFL production rate to 0. The *clv3* mutant was represented by setting the CLV3 protein production rate to 0. Each regulation-specific perturbation was modeled by setting the inhibition threshold to large number (1000). Because only qualitative information is available from the experimental data, we performed the fitting manually. To perform a simulation for a SAM system, we solved the system of ODEs numerically using the Tellurium package (Choi et al., 2018). The initial concentrations for all variables were set to zero. For all our analyses, steady-state solutions (at time unit 98) were used to determine the patterning of the SAM. For visualization of gene expression levels, expression values were normalized to [0, 1] by dividing each value by the maximum level of the molecule across all conditions.

Acknowledgements
We thank Jaydeep Kolape for training and technical assistance with confocal microscopy at Advanced Microscopy and Imaging Center, University of Tennessee, Knoxville. We thank Guangzhong Lin and Jijie Chai for sharing with us EPFL6 protein, and Ian Moore for sharing with us GR-LhG4:T35S, pBIN-LhGR-N and pH-TOP plasmids.

Competing interests
The authors declare no competing or financial interests.

Author contributions
Conceptualization: M.U., Z.L., L.Z., T.H., E.D.S.; Methodology: M.U., R.A.U.C., Z.L., A.M.O., D.D., L.Z.; Software: R.A.U.C., Z.L., T.H.; Validation: M.U., R.A.U.C., Z.L.; Formal analysis: M.U., R.A.U.C., Z.L., T.H., E.D.S.; Investigation: M.U., R.A.U.C., Z.L., A.M.O., D.D., L.Z., B.S.H., T.H., E.D.S.; Resources: A.M.O., D.D., L.Z.; Data curation: M.U., R.A.U.C.; Writing - original draft: M.U., R.A.U.C., Z.L., T.H., E.D.S.; Writing - review & editing: M.U., R.A.U.C., Z.L., A.M.O., D.D., L.Z., B.S.H., T.H., E.D.S.; Visualization: M.U., R.A.U.C., Z.L., D.D., T.H., E.D.S.; Supervision: T.H., E.D.S.; Project administration: T.H., E.D.S.; Funding acquisition: T.H., E.D.S.

Funding
This work was funded by the National Science Foundation (IOS–2016756 to E.D.S. and 2243562 to T.H.) and by the National Institutes of Health (R35GM149531 to T.H.). Deposited in PMC for release after 12 months.

Data availability
Code for reproducing the modeling result can be found at https://github.com/ZiyiiiLiu/SAM-model-3D. RNAseq data have been deposited in Gene Expression Omnibus under the accession GSE243494.

Peer review history
The peer review history is available online at https://journals.biologists.com/dev/lookup/doi/10.1242/dev.202870.reviewer-comments.pdf

References
Abrash, E. B., Davies, K. A. and Bergmann, D. C. (2011). Generation of signaling specificity in Arabidopsis by spatially restricted buffering of ligand–receptor interactions. *Plant Cell* **23**, 2864-2879. doi:10.1105/tpc.111.086637

Anderson, G. H., Alvarez, N. D. G., Gilman, C., Jeffares, D. C., Trainor, V. C. W., Hanson, M. R. and Veit, B. (2004). Diversification of genes encoding Mei2-like RNA binding proteins in plants. *Plant Mol. Biol.* **54**, 653-670. doi:10.1023/B:PLAN.0000040819.33383.b6

Bäurle, I. and Laux, T. (2005). Regulation of WUSCHEL transcription in the stem cell niche of the Arabidopsis shoot meristem. *Plant Cell* **17**, 2271-2280. doi:10.1105/tpc.105.032623

Brand, U., Fletcher, J. C., Hobe, M., Meyerowitz, E. M. and Simon, R. (2000). Dependence of stem cell fate in Arabidopsis on a feedback loop regulated by CLV3 activity. *Science* **289**, 617-619. doi:10.1126/science.289.5479.617

Capua, Y. and Eshed, Y. (2017). Coordination of auxin-triggered leaf initiation by tomato LEAFLESS. *Proc. Natl Acad. Sci. USA* **114**, 3246-3251. doi:10.1073/pnas.1617146114

Chandler, J. W. and Werr, W. (2014). Arabidopsis floral phytomer development: auxin response relative to biphasic modes of organ initiation. *J. Exp. Bot.* **65**, 3097-3110. doi:10.1093/jxb/eru153

Chandler, J. W., Cole, M., Flier, A., Grewe, B. and Werr, W. (2007). The AP2 transcription factors DORNRÖSCHEN and DORNRÖSCHEN-LIKE redundantly control Arabidopsis embryo patterning via interaction with PHAVOLUTA. *Development* **134**, 1653-1662. doi:10.1242/dev.001016

Chandler, J. W., Jacobs, B., Cole, M., Comelli, P. and Werr, W. (2011). DORNRÖSCHEN-LIKE expression marks Arabidopsis floral organ founder cells and precedes auxin response maxima. *Plant Mol. Biol.* **76**, 171-185. doi:10.1007/s11103-011-9779-8

Chen, M.-K., Wilson, R. L., Palme, K., Ditengou, F. A. and Shpak, E. D. (2013). ERECTA family genes regulate auxin transport in the shoot apical meristem and forming leaf primordia. *Plant Physiol.* **162**, 1978-1991. doi:10.1104/pp.113.218198

Chickarmane, V. S., Gordon, S. P., Tarr, P. T., Heisler, M. G. and Meyerowitz, E. M. (2012). Cytokinin signaling as a positional cue for patterning the apical–basal axis of the growing Arabidopsis shoot meristem. *Proc. Natl Acad. Sci. USA* **109**, 4002-4007. doi:10.1073/pnas.1200636109

Choi, K., Medley, J. K., König, M., Stocking, K., Smith, L., Gu, S. and Sauro, H. M. (2018). Tellurium: an extensible python-based modeling environment for systems and synthetic biology. *Biosystems* **171**, 74-79. doi:10.1016/j.biosystems.2018.07.006

Clark, S. E., Running, M. P. and Meyerowitz, E. M. (1993). CLAVATA1, a regulator of meristem and flower development in Arabidopsis. *Development* **119**, 397-418. doi:10.1242/dev.119.2.397

Clark, S. E., Running, M. P. and Meyerowitz, E. M. (1995). CLAVATA3 is a specific regulator of shoot and floral meristem development affecting the same processes as CLAVATA1. *Development* **121**, 2057-2067. doi:10.1242/dev.121.7.2057

Clough, S. J. and Bent, A. F. (1998). Floral dip: a simplified method for Agrobacterium-mediated transformation of Arabidopsis thaliana. *Plant J.* **16**, 735-743. doi:10.1046/j.1365-313x.1998.00343.x

Cole, M., Chandler, J., Weijers, D., Jacobs, B., Comelli, P. and Werr, W. (2009). DORNRÖSCHEN is a direct target of the auxin response factor MONOPTEROS in the Arabidopsis embryo. *Development* **136**, 1643-1651. doi:10.1242/dev.032177

Comelli, P., Glowa, D., Chandler, J. W. and Werr, W. (2016). Founder-cell-specific transcription of the DORNRÖSCHEN-LIKE promoter and integration of the auxin response. *J. Exp. Bot.* **67**, 143-155. doi:10.1093/jxb/erv442

Dai, Y., Luo, L. and Zhao, Z. (2023). Genetic robustness control of auxin output in priming organ initiation. *Proc. Natl Acad. Sci. USA* **120**, e2221606120. doi:10.1073/pnas.2221606120

Dao, T. Q., Weksler, N., Liu, H. M.-H., Leiboff, S. and Fletcher, J. C. (2022). Interactive CLV3, CLE16 and CLE17 signaling mediates stem cell homeostasis in the Arabidopsis shoot apical meristem. *Development* **149**, dev200787. doi:10.1242/dev.200787

Daum, G., Medzihradszky, A., Suzaki, T. and Lohmann, J. U. (2014). A mechanistic framework for noncell autonomous stem cell induction in Arabidopsis. *Proc. Natl. Acad. Sci. USA* **111**, 14619-14624. doi:10.1073/pnas.1406446111

Degennaro, D., Urquidi Camacho, R. A., Zhang, L. and Shpak, E. D. (2022). Initiation of aboveground organ primordia depends on combined action of auxin, ERECTA family genes, and PINOID. *Plant Physiol.* **190**, 794-812. doi:10.1093/plphys/kiac288

Delile, J., Herrmann, M., Peyriéras, N. and Doursat, R. (2017). A cell-based computational model of early embryogenesis coupling mechanical behaviour and gene regulation. *Nat. Commun.* **8**, 1-10. doi:10.1038/ncomms13929

Demesa-Arevalo, E., Narasimhan, M. and Simon, R. (2024). Intercellular communication in shoot meristems. *Annu. Rev. Plant Biol.* **75**, 23.1-23.26. doi:10.1146/annurev-arplant-070523-035342

Dobin, A., Davis, C. A., Schlesinger, F., Drenkow, J., Zaleski, C., Jha, S., Batut, P., Chaisson, M. and Gingeras, T. R. (2013). STAR: ultrafast universal RNA-seq aligner. *Bioinformatics* **29**, 15-21. doi:10.1093/bioinformatics/bts635

Fletcher, J. C., Brand, U., Running, M. P., Simon, R. and Meyerowitz, E. M. (1999). Signaling of cell fate decisions by CLAVATA3 in Arabidopsis shoot meristems. *Science* **283**, 1911-1914. doi:10.1126/science.283.5409.1911

Fouracre, J. P. and Harrison, C. J. (2022). How was apical growth regulated in the ancestral land plant? Insights from the development of non-seed plants. *Plant Physiol.* **190**, 100-112. doi:10.1093/plphys/kiac313

Fuchs, M. and Lohmann, J. U. (2020). Aiming for the top: non-cell autonomous control of shoot stem cells in Arabidopsis. *J. Plant Res.* **133**, 297-309. doi:10.1007/s10265-020-01174-3

Fujihara, R., Uchida, N., Tameshige, T., Kawamoto, N., Hotokezaka, Y., Higaki, T., Simon, R., Torii, K. U., Tasaka, M. and Aida, M. (2021). The boundary-expressed EPIDERMAL PATTERNING FACTOR-LIKE2 gene encoding a signaling peptide promotes cotyledon growth during Arabidopsis thaliana embryogenesis. *Plant Biotechnol. (Tokyo)* **38**, 317-322. doi:10.5511/plantbiotechnology.21.0508a

Fujita, H., Toyokura, K., Okada, K. and Kawaguchi, M. (2011). Reaction-diffusion pattern in shoot apical meristem of plants. *PLoS ONE* **6**, e18243. doi:10.1371/journal.pone.0018243

Gordon, S. P., Chickarmane, V. S., Ohno, C. and Meyerowitz, E. M. (2009). Multiple feedback loops through cytokinin signaling control stem cell number within the Arabidopsis shoot meristem. *Proc. Natl. Acad. Sci. USA* **106**, 16529-16534. doi:10.1073/pnas.0908122106

Gruel, J., Landrein, B., Tarr, P., Schuster, C., Refahi, Y., Sampathkumar, A., Hamant, O., Meyerowitz, E. M. and Jönsson, H. (2016). An epidermis-driven mechanism positions and scales stem cell niches in plants. *Sci. Adv.* **2**, e1500989. doi:10.1126/sciadv.1500989

Gruel, J., Deichmann, J., Landrein, B., Hitchcock, T. and Jönsson, H. (2018). The interaction of transcription factors controls the spatial layout of plant aerial stem cell niches. *NPJ Syst. Biol. Appl.* **4**, 36. doi:10.1038/s41540-018-0072-1

Hajdukiewicz, P., Svab, Z. and Maliga, P. (1994). The small, versatile pPZP family of Agrobacterium binary vectors for plant transformation. *Plant Mol. Biol.* **25**, 989-994. doi:10.1007/BF00014672

Han, H., Liu, X. and Zhou, Y. (2020a). Transcriptional circuits in control of shoot stem cell homeostasis. *Curr. Opin. Plant Biol.* **53**, 50-56. doi:10.1016/j.pbi.2019.10.004

Han, H., Yan, A., Li, L., Zhu, Y., Feng, B., Liu, X. and Zhou, Y. (2020b). A signal cascade originated from epidermis defines apical-basal patterning of Arabidopsis shoot apical meristems. *Nat. Commun.* **11**, 1-17. doi:10.1038/s41467-020-14989-4

He, Y., He, X., Wang, X., Hao, M., Gao, J., Wang, Y., Yang, Z.-N. and Meng, X. (2023). An EPFL peptide signaling pathway promotes stamen elongation via enhancing filament cell proliferation to ensure successful self-pollination in Arabidopsis thaliana. *New Phytol.* **238**, 1045-1058. doi:10.1111/nph.18806

Hirakawa, Y. (2021). CLAVATA3, a plant peptide controlling stem cell fate in the meristem. *Peptides* **142**, 170579. doi:10.1016/j.peptides.2021.170579

Hirakawa, Y., Fujimoto, T., Ishida, S., Uchida, N., Sawa, S., Kiyosue, T., Ishizaki, K., Nishihama, R., Kohchi, T. and Bowman, J. L. (2020). Induction of multichotomous branching by CLAVATA peptide in Marchantia polymorpha. *Curr. Biol.* **30**, 3833-3840.e4. doi:10.1016/j.cub.2020.07.016

Hohm, T., Zitzler, E. and Simon, R. (2010). A dynamic model for stem cell homeostasis and patterning in Arabidopsis meristems. *PLoS ONE* **5**, e9189. doi:10.1371/journal.pone.0009189

Hu, C., Zhu, Y., Cui, Y., Cheng, K., Liang, W., Wei, Z., Zhu, M., Yin, H., Zeng, L., Xiao, Y. et al. (2018). A group of receptor kinases are essential for CLAVATA signalling to maintain stem cell homeostasis. *Nat. Plants* **4**, 205-211. doi:10.1038/s41477-018-0123-z

Huang, Y., Tao, Z., Liu, Q., Wang, X., Yu, J., Liu, G. and Wang, H. (2014). BnEPFL6, an EPIDERMAL PATTERNING FACTOR-LIKE (EPFL) secreted peptide gene, is required for filament elongation in Brassica napus. *Plant Mol. Biol.* **85**, 505-517. doi:10.1007/s11103-014-0200-2

Ikeda, Y., Banno, H., Niu, Q.-W., Howell, S. H. and Chua, N.-H. (2006). The ENHANCER OF SHOOT REGENERATION 2 gene in Arabidopsis regulates CUP-SHAPED COTYLEDON 1 at the transcriptional level and controls cotyledon development. *Plant Cell Physiol.* **47**, 1443-1456. doi:10.1093/pcp/pcl023

Ikeda, Y., Králová, M., Zalabák, D., Kubalová, I. and Aida, M. (2021). Post-Embryonic Lateral Organ Development and Adaxial—Abaxial Polarity Are Regulated by the Combined Effect of ENHANCER OF SHOOT REGENERATION 1 and WUSCHEL in Arabidopsis Shoots. *Int. J. Mol. Sci.* **22**, 10621. doi:10.3390/ijms221910621

Ince, Y. Ç. and Sugimoto, K. (2023). Illuminating the path to shoot meristem regeneration: Molecular insights into reprogramming cells into stem cells. *Curr. Opin. Plant Biol.* **76**, 102452. doi:10.1016/j.pbi.2023.102452

Je, B. I., Gruel, J., Lee, Y. K., Bommert, P., Arevalo, E. D., Eveland, A. L., Wu, Q., Goldshmidt, A., Meeley, R., Bartlett, M. et al. (2016). Signaling from maize organ primordia via FASCIATED EAR3 regulates stem cell proliferation and yield traits. *Nat. Genet.* **48**, 785-791. doi:10.1038/ng.3567

Kawakatsu, T., Itoh, J.-I., Miyoshi, K., Kurata, N., Alvarez, N., Veit, B. and Nagato, Y. (2006). PLASTOCHRON2 regulates leaf initiation and maturation in rice. *Plant Cell* **18**, 612-625. doi:10.1105/tpc.105.037622

Kawamoto, N., DEL Carpio, D. P., Hofmann, A., Mizuta, Y., Kurihara, D., Higashiyama, T., Uchida, N., Torii, K. U., Colombo, L., Groth, G. and et al. (2020). A peptide pair coordinates regular ovule initiation patterns with seed number and fruit size. *Curr. Biol.* **30**, 4352-4361.e4. doi:10.1016/j.cub.2020.08.050

Kimura, Y., Tasaka, M., Torii, K. U. and Uchida, N. (2018). ERECTA-family genes coordinate stem cell functions between the epidermal and internal layers of the shoot apical meristem. *Development* **145**, dev156380. doi:10.1242/dev.156380

Kirch, T., Simon, R. D., Grünewald, M. and Werr, W. (2003). The DORNRÖSCHEN/ENHANCER OF SHOOT REGENERATION1 gene of Arabidopsis acts in the control of meristem cell fate and lateral organ development. *Plant Cell* **15**, 694-705. doi:10.1105/tpc.009480

Kosentka, P. Z., Overholt, A., Maradiaga, R., Mitoubsi, O. and Shpak, E. D. (2019). EPFL signals in the boundary region of the SAM restrict its size and promote leaf initiation. *Plant Physiol.* **179**, 265. doi:10.1104/pp.18.00714

Kurihara, D., Mizuta, Y., Sato, Y. and Higashiyama, T. (2015). ClearSee: a rapid optical clearing reagent for whole-plant fluorescence imaging. *Development* **142**, 4168-4179. doi:10.1242/dev.127613

Kusnandar, A. S., Itoh, J.-I., Sato, Y., Honda, E., Hibara, K.-I., Kyozuka, J. and Naramoto, S. (2021). NARROW AND DWARF LEAF 1, the Ortholog of Arabidopsis ENHANCER OF SHOOT REGENERATION1/Dornröschen, Mediates Leaf Development and Maintenance of the Shoot Apical Meristem in Oryza sativa L. *Plant Cell Physiol.* **63**, 265-278. doi:10.1093/pcp/pcab169

Laux, T., Mayer, K. F. X., Berger, J. and Jurgens, G. (1996). The WUSCHEL gene is required for shoot and floral meristem integrity in Arabidopsis. *Development* **122**, 87-96. doi:10.1242/dev.122.1.87

Lee, J. S., Hnilova, M., Maes, M., Lin, Y.-C. L., Putarjunan, A., Han, S.-K., Avila, J. and Torii, K. U. (2015). Competitive binding of antagonistic peptides fine-tunes stomatal patterning. *Nature* **522**, 439-443. doi:10.1038/nature14561

Leibfried, A., To, J. P. C., Busch, W., Stehling, S., Kehle, A., Demar, M., Kieber, J. J. and Lohmann, J. U. (2005). WUSCHEL controls meristem function by direct regulation of cytokinin-inducible response regulators. *Nature* **438**, 1172. doi:10.1038/nature04270

Lenhard, M. and Laux, T. (2003). Stem cell homeostasis in the Arabidopsis shoot meristem is regulated by intercellular movement of CLAVATA3 and its sequestration by CLAVATA1. *Development* **130**, 3163-3173. doi:10.1242/dev.00525

Liao, Y., Smyth, G. K. and Shi, W. (2013). featureCounts: an efficient general purpose program for assigning sequence reads to genomic features. *Bioinformatics* **30**, 923-930. doi:10.1093/bioinformatics/btt656

Lin, G., Zhang, L., Han, Z., Yang, X., Liu, W., Li, E., Chang, J., Qi, Y., Shpak, E. D. and Chai, J. (2017). A receptor-like protein acts as a specificity switch for the regulation of stomatal development. *Genes Dev.* **31**, 927-938. doi:10.1101/gad.297580.117

Lindsay, D. L., Sawhney, V. K. and Bonham-Smith, P. C. (2006). Cytokinin-induced changes in CLAVATA1 and WUSCHEL expression temporally coincide with altered floral development in Arabidopsis. *Plant Sci.* **170**, 1111-1117. doi:10.1016/j.plantsci.2006.01.015

Liu, Z., Shpak, E. D. and Hong, T. (2020). A mathematical model for understanding synergistic regulations and paradoxical feedbacks in the shoot apical meristem. *Comput. Struct. Biotechnol. J.* **18**, 3877-3889. doi:10.1016/j.csbj.2020.11.017

Livak, K. J. and Schmittgen, T. D. (2001). Analysis of relative gene expression data using real-time quantitative PCR and the 2DDC(T) method. *Methods* **25**, 402-408. doi:10.1006/meth.2001.1262

Long, J. A. and Barton, M. K. (1998). The development of apical embryonic pattern in Arabidopsis. *Development* **125**, 3027-3035. doi:10.1242/dev.125.16.3027

Lopes, F. L., Galvan-Ampudia, C. and Landrein, B. (2021). WUSCHEL in the shoot apical meristem: old player, new tricks. *J. Exp. Bot.* **72**, 1527-1535. doi:10.1093/jxb/eraa572

Love, M. I., Huber, W. and Anders, S. (2014). Moderated estimation of fold change and dispersion for RNA-seq data with DESeq2. *Genome Biol.* **15**, 550. doi:10.1186/s13059-014-0550-8

Luo, L., Zeng, J., Wu, H., Tian, Z. and Zhao, Z. (2018). A molecular framework for auxin-controlled homeostasis of shoot stem cells in Arabidopsis. *Mol. Plant* **11**, 899-913. doi:10.1016/j.molp.2018.04.006

Mandel, T., Moreau, F., Kutsher, Y., Fletcher, J. C., Carles, C. C. and Williams, L. E. (2014). The ERECTA receptor kinase regulates Arabidopsis shoot apical meristem size, phyllotaxy and floral meristem identity. *Development* **141**, 830-841. doi:10.1242/dev.104687

Mayer, K. F. X., Schoof, H., Haecker, A., Lenhard, M., Jürgens, G. and Laux, T. (1998). Role of WUSCHEL in regulating stem cell fate in the Arabidopsis shoot meristem. *Cell* **95**, 805-815. doi:10.1016/S0092-8674(00)81703-1

Musielak, T. J., Schenkel, L., Kolb, M., Henschen, A. and Bayer, M. (2015). A simple and versatile cell wall staining protocol to study plant reproduction. *Plant Reprod.* **28**, 161-169. doi:10.1007/s00497-015-0267-1

Nag, A., Yang, Y. and Jack, T. (2007). DORNRÖSCHEN-Like, an AP2 gene, is necessary for stamen emergence in Arabidopsis. *Plant Mol. Biol.* **65**, 219-232. doi:10.1007/s11103-007-9210-7

Narasimhan, M. and Simon, R. (2022). Spatial range, temporal span, and promiscuity of CLE-RLK signaling. *Front. Plant Sci.* **13**, 906087. doi:10.3389/fpls.2022.906087

Nardmann, J. and Werr, W. (2012). The invention of WUS-like stem cell-promoting functions in plants predates leptosporangiate ferns. *Plant Mol. Biol.* **78**, 123-134. doi:10.1007/s11103-011-9851-4

Negoro, S., Hirabayashi, T., Iwasaki, R., Torii, K. U. and Uchida, N. (2023). EPFL peptide signalling ensures robust self-pollination success under cool temperature stress by aligning the length of the stamen and pistil. *Plant Cell Environ.* **46**, 451-463. doi:10.1111/pce.14498

Nikolaev, S. V., Penenko, A. V., Lavreha, V. V., Mjolsness, E. D. and Kolchanov, N. A. (2007). A model study of the role of proteins CLV1, CLV2, CLV3, and WUS in regulation of the structure of the shoot apical meristem. *Russian J. Dev. Biol.* **38**, 383-388. doi:10.1134/S1062360407060069

Nimchuk, Z. L., Zhou, Y., Tarr, P. T., Peterson, B. A. and Meyerowitz, E. M. (2015). Plant stem cell maintenance by transcriptional cross-regulation of related receptor kinases. *Development* **142**, 1043-1049. doi:10.1242/dev.119677

Ohki, S., Takeuchi, M. F. and Mori, M. (2011). The NMR structure of stomagen reveals the basis of stomatal density regulation by plant peptide hormones. *Nat. Commun.* **2**, 512. doi:10.1038/ncomms1520

Perales, M., Rodriguez, K., Snipes, S., Yadav, R. K., Diaz-Mendoza, M. and Reddy, G. V. (2016). Threshold-dependent transcriptional discrimination underlies stem cell homeostasis. *Proc. Natl. Acad. Sci. USA* **113**, E6298-E6306. doi:10.1073/pnas.1607669113

Pillitteri, L. J., Bemis, S. M., Shpak, E. D. and Torii, K. U. (2007). Haploinsufficiency after successive loss of signaling reveals a role for ERECTA-family genes in Arabidopsis ovule development. *Development* **134**, 3099-3109. doi:10.1242/dev.004788

Reddy, G. V. and Meyerowitz, E. M. (2005). Stem-cell homeostasis and growth dynamics can be uncoupled in the Arabidopsis shoot apex. *Science* **310**, 663-667. doi:10.1126/science.1116261

Richardson, L. G. L. and Torii, K. U. (2013). Take a deep breath: peptide signalling in stomatal patterning and differentiation. *J. Exp. Bot.* **64**, 5243-5251. doi:10.1093/jxb/ert246

Samalova, M., Brzobohaty, B. and Moore, I. (2005). pOp6/LhGR: a stringently regulated and highly responsive dexamethasone-inducible gene expression system for tobacco. *Plant J.* **41**, 919-935. doi:10.1111/j.1365-313X.2005.02341.x

Schindelin, J., Arganda-Carreras, I., Frise, E., Kaynig, V., Longair, M., Pietzsch T., et al. (2012) Fiji: an open-source platform for biological-image analysis. *Nat. Methods* **9**, 676-682. doi:10.1038/nmeth.2019

Schlegel, J., Denay, G., Wink, R., Pinto, K. G., Stahl, Y., Schmid, J., Blümke, P. and Simon, R. G. (2021). Control of Arabidopsis shoot stem cell homeostasis by two antagonistic CLE peptide signalling pathways. *eLife* **10**, e70934. doi:10.7554/eLife.70934.sa2

Schoof, H., Lenhard, M., Haecker, A., Mayer, K. F. X., Jurgens, G. and Laux, T. (2000). The stem cell population of Arabidopsis shoot meristems is maintained by a regulatory loop between the CLAVATA and WUSCHEL genes. *Cell* **100**, 635-644. doi:10.1016/S0092-8674(00)80700-X

Shimotohno, A. (2022). Illuminating the molecular mechanisms underlying shoot apical meristem homeostasis in plants. *Plant Biotechnol. (Tokyo)* **39**, 19-28. doi:10.5511/plantbiotechnology.22.0213a

Shimotohno, A. and Scheres, B. (2019). Topology of regulatory networks that guide plant meristem activity: similarities and differences. *Curr. Opin. Plant Biol.* **51**, 74-80. doi:10.1016/j.pbi.2019.04.006

Shpak, E. D., Berthiaume, C. T., Hill, E. J. and Torii, K. U. (2004). Synergistic interaction of three ERECTA-family receptor-like kinases controls Arabidopsis organ growth and flower development by promoting cell proliferation. *Development* **131**, 1491-1501. doi:10.1242/dev.01028

Stephens, M. (2017). False discovery rates: a new deal. *Biostatistics* **18**, 275-294. doi:10.1101/038216

Takata, N., Yokota, K., Ohki, S., Mori, M., Taniguchi, T. and Kurita, M. (2013). Evolutionary Relationship and Structural Characterization of the EPF/EPFL Gene Family. *PLoS ONE* **8**, e65183. doi:10.1371/journal.pone.0065183

Tameshige, T., Okamoto, S., Lee, J. S., Aida, M., Tasaka, M., Torii, K. U. and Uchida, N. (2016). A secreted peptide and its receptors shape the auxin response pattern and leaf margin morphogenesis. *Curr. Biol.* **26**, 2478-2485. doi:10.1016/j.cub.2016.07.014

To, J. P. C., Haberer, G., Ferreira, F. J., Deruere, J., Mason, M. G., Schaller, G. E., Alonso, J. M., Ecker, J. R. and Kieber, J. J. (2004). Type-A Arabidopsis response regulators are partially redundant negative regulators of cytokinin signaling. *Plant Cell* **16**, 658-671. doi:10.1105/tpc.018978

Truskina, J. and Vernoux, T. (2018). The growth of a stable stationary structure: coordinating cell behavior and patterning at the shoot apical meristem. *Curr. Opin. Plant Biol.* **41**, 83-88. doi:10.1016/j.pbi.2017.09.011

Uchida, N. and Torii, K. U. (2019). Stem cells within the shoot apical meristem: identity, arrangement and communication. *Cell. Mol. Life Sci.* **76**, 1067-1080. doi:10.1007/s00018-018-2980-z

Uchida, N., Lee, J. S., Horst, R. J., Lai, H.-H., Kajita, R., Kakimoto, T., Tasaka, M. and Torii, K. U. (2012a). Regulation of inflorescence architecture by intertissue layer ligand–receptor communication between endodermis and phloem. *Proc. Natl. Acad. Sci. USA* **109**, 6337-6342. doi:10.1073/pnas.1117537109

Uchida, N., Shimada, M. and Tasaka, M. (2012b). Modulation of the balance between stem cell proliferation and consumption by ERECTA-family genes. *Plant Signal. Behav.* **7**, 1506-1508. doi:10.4161/psb.22080

Uchida, N., Shimada, M. and Tasaka, M. (2013). ERECTA-family receptor kinases regulate stem cell homeostasis via buffering its cytokinin responsiveness in the shoot apical meristem. *Plant Cell Physiol.* **54**, 343-351. doi:10.1093/pcp/pcs109

Veit, B., Briggs, S. P., Schmidt, R. J., Yanofsky, M. F. and Hake, S. (1998). Regulation of leaf initiation by the terminal ear 1 gene of maize. *Nature* **393**, 166-168. doi:10.1038/30239

Vivancos, J., Spinner, L., Mazubert, C., Charlot, F., Paquet, N., Thareau, V., Dron, M., Nogué, F. and Charon, C. (2012). The function of the RNA-binding protein TEL1 in moss reveals ancient regulatory mechanisms of shoot development. *Plant Mol. Biol.* **78**, 323-336. doi:10.1007/s11103-011-9867-9

Wang, Y. (2021). Stem cell basis for fractal patterns: axillary meristem initiation. *Front. Plant Sci.* **12**, 805434. doi:10.3389/fpls.2021.805434

Wang, L., Wang, S. and Li, W. (2012). RSeQC: quality control of RNA-seq experiments. *Bioinformatics* **28**, 2184-2185. doi:10.1093/bioinformatics/bts356

Wang, J., Tian, C., Zhang, C., Shi, B., Cao, X., Zhang, T.-Q., Zhao, Z., Wang, J.-W. and Jiao, Y. (2017). Cytokinin signaling activates WUSCHEL expression during axillary meristem initiation. *Plant Cell* **29**, 1373-1387. doi:10.1105/tpc.16.00579

Wenzl, C. and Lohmann, J. U. (2023). 3D imaging reveals apical stem cell responses to ambient temperature. *Cells Dev.* **175**, 203850. doi:10.1016/j.cdev.2023.203850

Xiong, G. S., Hu, X. M., Jiao, Y. Q., Yu, Y. C., Chu, C. C., Li, J. Y., Qian, Q. and Wang, Y. H. (2006). Leafy head2, which encodes a putative RNA-binding protein, regulates shoot development of rice. *Cell Res.* **16**, 267-276. doi:10.1038/sj.cr.7310034

Yadav, R. K., Girke, T., Pasala, S., Xie, M. and Reddy, G. V. (2009). Gene expression map of the Arabidopsis shoot apical meristem stem cell niche. *Proc. Natl. Acad. Sci. USA* **106**, 4941-4946. doi:10.1073/pnas.0900843106

Yadav, R. K., Tavakkoli, M. and Reddy, G. V. (2010). WUSCHEL mediates stem cell homeostasis by regulating stem cell number and patterns of cell division and differentiation of stem cell progenitors. *Development* **137**, 3581-3589. doi:10.1242/dev.054973

Yadav, R. K., Perales, M., Gruel, J., Girke, T., Jönsson, H. and Reddy, G. V. (2011). WUSCHEL protein movement mediates stem cell homeostasis in the Arabidopsis shoot apex. *Genes Dev.* **25**, 2025-2030. doi:10.1101/gad.17258511

Yadav, R. K., Perales, M., Gruel, J., Ohno, C., Heisler, M., Girke, T., Jönsson, H. and Reddy, G. V. (2013). Plant stem cell maintenance involves direct transcriptional repression of differentiation program. *Mol. Syst. Biol.* **9**, 654. doi:10.1038/msb.2013.8

Ye, Y., Kang, X., Bailey, J., Li, C. and Hong, T. (2019). An enriched network motif family regulates multistep cell fate transitions with restricted reversibility. *PLoS Comput. Biol.* **15**, e1006855. doi:10.1371/journal.pcbi.1006855

Zhang, T.-Q., Lian, H., Zhou, C.-M., Xu, L., Jiao, Y. and Wang, J.-W. (2017). A two-step model for de novo activation of WUSCHEL during plant shoot regeneration. *Plant Cell* **29**, 1073-1087. doi:10.1105/tpc.16.00863

Zhang, L., Degennaro, D., Lin, G., Chai, J. and Shpak, E. D. (2021). ERECTA family signaling constrains CLAVATA3 and WUSCHEL to the center of the shoot apical meristem. *Development* **148**, dev189753. doi:10.1242/dev.189753

Zhou, Y., Yan, A., Han, H., Li, T., Geng, Y., Liu, X. and Meyerowitz, E. M. (2018). HAIRY MERISTEM with WUSCHEL confines CLAVATA3 expression to the outer apical meristem layers. *Science* **361**, 502-506. doi:10.1126/science.aar8638